Multi-Objective Assessment of Hydrogen Energy Systems for Residential PV Integration in Power-to-Power and Power-to-Gas Applications: A Comparative Life Cycle Assessment across European Energy Mixes

Mathieu PATIN[1,2a], Sylvie BEGOT[1], Frédéric GUSTIN[1], Valérie LEPILLER[1]

[1]Université de Franche-Comté, FEMTO-ST, FCLAB, UTBM, CNRS, Belfort, France

[2]Univ. Grenoble Alpes, CEA, Liten, DTCH, 38000, Grenoble, France

[a]mathieu.patin@cea.fr, 50 avenue du Lac Léman, 73370 Le Bourget du Lac, France

Abstract

The building sector is one of the most energy-intensive sectors globally, and photovoltaic (PV) energy is widely adopted to meet residential energy demand in a low-carbon manner. However, the mismatch between PV production and household demand often leads to periods of surplus energy. This study aims to evaluate the potential of hydrogen-based energy systems to capitalize on this excess energy. To achieve this, a model that generates consistent, continuous, and diverse electrical and thermal load profiles for low-carbon residential buildings is coupled with a multi-energy system simulation. The simulation computes the performance of hydrogen components for different hydrogen utilization (Power-to-Power and Power-to-Gas) and energy mix configurations. The systems' energy, economic, and emission performance are analyzed using a multi-objective optimization process to evaluate their competitiveness and identify optimal sizing strategies. The results show that system performance varies significantly depending on the criteria, usage, and energy mix of the electrical grid. For Power-to-Power applications (using hydrogen to produce electricity and heat), the system excels in providing renewable energy but is not cost-competitive with the French electricity grid, nor does it significantly reduce emissions. However, it proves competitive in terms of life-cycle emissions considering most European energy mixes. For Power-to-Gas applications (producing hydrogen for sale), the hydrogen production is not economically competitive without subsidies but shows potential for reducing emissions, especially in carbon-intensive sectors like transport and industry.

Graphical abstract

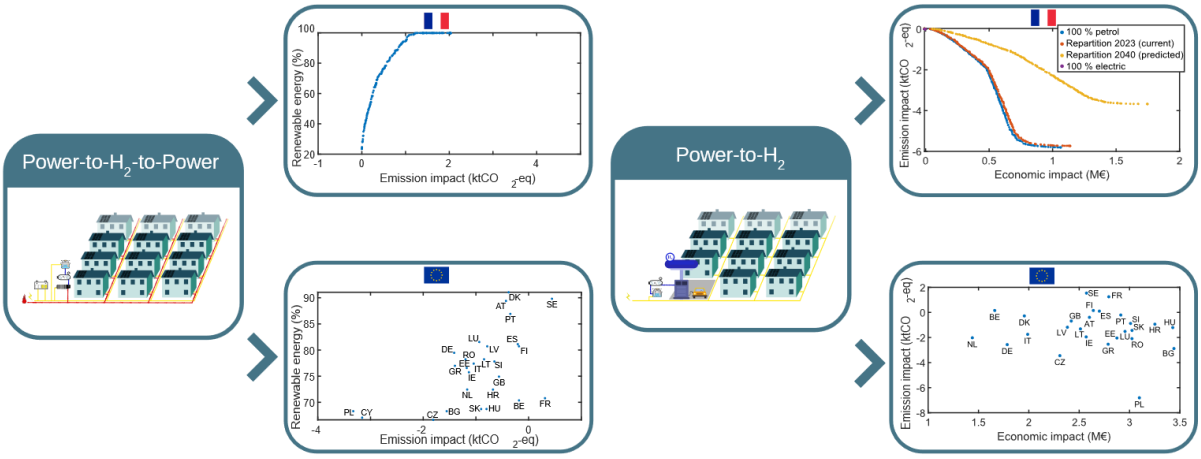

Highlights

* Multi-objective and multi-use optimization of residential hydrogen-based systems

* Multi-indicators study of the performances' variations across European energy mixes

* Residential Power-to-Power hydrogen systems struggle compared to a decarbonized grid

* Power-to-Gas systems are competitive emission-wise for transport and industry use

* Power-to-Gas systems enable greater emission reductions compared to Power-to-Power

Keywords: Hydrogen-energy, Multi-objective optimization, Power-to-Power, Power-to-Gas, Life cycle assessment, Multi-energy system, Residential load modeling

Nomenclature

Symbols

C	Cost (€)
Em	Greenhouse gas emission ($kgCO_2eq$)
E	Energy (kWh)
fr	Fraction
G	Gain (€)
HHV	Higher Heating Value (J/kg)
L	Scaling factor
M	Molar mass (kg/mol)
$\dot{m}$	Mass flow rate (kg/s)

N	Compressor stage number
Ob	Objective
P	Power (W)
Pr	Pressure (Pa)
Q	Energy capacity of the battery (kWh)
R	Universal gas constant (J/mol/K)
S	Size (m^2, kWh, kW or kg_{H2})
t	time (minute)
tx	rate
T	Temperature (K)
W	Specific Work (J/kg)
y	year
Z	Compressibility factor
γ	Heat capacity ratio
η	Efficiency

Indices

ab	Absorbed
av	Avoided
ba	Battery
by	Buy
ch	Charge
cp	Compressor
cs	Consume
dm	Demande
di	Discharge
dc	Discount
e	Energy
el	Electrical
en	Environmental

gr	Grid
H_2	Dihydrogen
he	Heating
if	Inflation
in	Input
it	Initial
is	Isentropic
iv	Investment
lt	Lifetime
max	Maximum
min	Minimum
mt	Motor
nm	Nominal
out	Output
pd	Produced
pr	Provided
r	Real
rf	Reference
rm	Replacement
rt	Rest
sl	Sold
sys	System
th	Thermal
tt	Total
y	Year

Abbreviations

COP	Coefficient Of Performance
CRF	Capital recovery factor
DHW	Domestic Hot Water

DOD	Depth of Discharge
EC	Electrolyzer
EV	Electric Vehicle
FC	Fuel Cell
LCA	Life Cycle Assessment
O&M	Operation and Maintenance
PV	Photovoltaics
PEM	Proton Exchange Membrane
REP	Renewable energy proportion
SOC	State Of Charge

1. Introduction

Climate change is a global challenge requiring urgent, coordinated action. The building sector, responsible for roughly 30% of global final energy consumption, is among the most energy-intensive [1]. Addressing climate change challenges must therefore include efforts to reduce energy consumption in this sector and to transition away from high-carbon energy sources such as natural gas.

Renewable energy, particularly solar photovoltaic (PV) systems, has become a widely adopted solution for residential buildings due to the availability of large roof surfaces. However, PV generation is intermittent and temporally misaligned with demand, often producing surplus electricity during daylight hours. Strategies to utilize this excess production are critical. This study focuses on hydrogen-based solutions for residential applications.

In such multi-energy systems, excess PV electricity can be used to power a water electrolyzer (EC) to produce hydrogen, which can be utilized in two main ways. In Power-to-Power applications, hydrogen is converted back into electricity and heat during periods of low solar generation. In contrast, Power-to-Gas applications use hydrogen in non-energy sectors, such as transportation (e.g., hydrogen vehicles) or industrial chemical processes. Hydrogen-based systems can be applied across various scales and usage scenarios, offering flexibility for different energy needs.

In Power-to-Power applications, a fuel cell (FC) is typically used to convert stored hydrogen back into electricity, allowing the system to function as an energy storage solution, similar to a battery. A fuel cell can produce both electricity and heat, although some studies focus exclusively on electricity generation. For instance, Mansir et al. investigate a hydrogen-based system designed to meet the electricity demand of a residential building, while heat is supplied using a gas boiler and gas turbine [2].

Mohammed et al. modeled a similar system to meet residential electricity demand, optimizing for cost and reliability; environmental impacts were assessed but not used in optimization [3]. The system is dimensioned with two objectives in mind: minimizing total system cost and maximizing reliability. Although an environmental indicator is calculated, it is not used in the optimization process. Their results indicate that the system, while not economically attractive, offers good reliability and notable emission reductions.

In another study, Ghenai et al. investigate a hydrogen-based system designed to meet the total energy demand of 150 houses in a desert region [4]. Here, hydrogen is partially produced from locally generated excess photovoltaic electricity, with additional imports as needed. The system is optimized by evaluating the economic performance of various fixed-size component combinations. The study concludes that the system is capable of meeting the annual load at a cost of 0.145 $/kWh, demonstrating competitiveness with conventional energy systems.

Monforti Ferrario et al. optimized a microgrid with PV and wind for a 14-apartment building in Spain, comparing hybrid battery-hydrogen storage with hydrogen-only systems [5]. Multiple system designs were optimized based on total system cost, overall efficiency, and energy supply security. The comparison of the designs revealed that hybridizing battery storage with hydrogen storage improves energy security compared to hydrogen storage alone, but at the expense of significantly higher system costs.

Babatunde et al. compared four systems, with and without hydrogen components, to meet the electricity demand of a residence in Nigeria [6]. The configurations were evaluated using six criteria: three economic (total investment cost, total discounted cost, and energy cost), two technical (load deficit and energy surplus), and one environmental (NOx emissions during operation). The study found that systems without hydrogen were more economically efficient, but those with hydrogen performed better when evaluated using multiple criteria.

Kilic and Altun studied a hydrogen storage system for a building in Turkey, modelling several configurations based on discounted energy cost and annual system emissions associated with a backup diesel generator [7]. They concluded that battery-based systems performed better than hydrogen storage in terms of cost, but the limited storage capacity of batteries led to higher diesel consumption. Hydrogen storage resulted in lower emissions but was less economical compared to diesel-only systems.

It can be estimated that approximately 50% of the energy used by a fuel cell is converted into electricity, with the other 50% lost as heat [8]. Utilizing this waste heat can enhance the system's energy performance. One approach is to use the generated heat as an energy source for other systems producing electricity. Zhao et al. specifically study the integration of a proton exchange membrane fuel cell with an organic Rankine cycle [9]. In their system, the waste heat from the fuel cell serves as a heat source for the thermodynamic cycle, which generates additional electricity via a turbine. Other studies focus on recovering this heat to directly improve the efficiency of the fuel cell stack itself. This is the case with Nguyen et al., who use the heat generated to improve performance in cold climates [10]. In cold climates, preheating the intake air is necessary to reduce the likelihood of ice formation. Additionally, the heat can be utilized for cooling purposes. For example, Lambert et al. combine fuel cells with an adsorption cooling system [15]. The heat from the fuel cell is used to assist a cycle of ammonia storage and release in a refrigeration system [11]. In residential applications, a common use of fuel cell waste heat is in combined heat and power (CHP) systems.

Cikatić Šanić and Barbir designed a hydrogen storage system to meet the electricity, heating, and cooling demands of a dwelling in Croatia [12]. Hosseini et al. investigated the energy and exergy efficiency of a micro-CHP system for a single-family home in Canada, operating in off-grid conditions [13] In both cases, the waste heat from the fuel cell was used to meet heating and hot water demands.

At a district scale, cogeneration can be implemented through district heating networks. Gabrielli et al. optimized a hydrogen-based system for a small district consisting of 24 buildings, including residential and commercial/office buildings, using two criteria: cost and CO2 emissions [14, 15]. Their results showed that the optimal configuration for minimizing emissions involved a system with both a fuel cell and a battery. However, hydrogen-based systems underperformed in terms of cost.

Mustafa et al. proposed a system using hydrogen storage system to meet the electrical and thermal demands of 100 homes in Saudi Arabia [16]. The system was sized based on economic indicators using Homer® software, with environmental considerations incorporated through an economic penalty. The study concluded that the system is not economically competitive under current conditions (interest rates and emission penalties) but could become viable under stricter CO_2 emission pricing policies.

Eldakadosi and Schneeloch optimized a hydrogen-based system to produce electricity and heat for a German residential district using excess PV production [17]. The system was optimized based on total cost and operational emissions. When compared with a gas boiler and heat pump system, the authors found that the hydrogen-based system performed better in terms of emissions but was less cost-effective.

For residential Power-to-Gas applications, Fambri et al. conducted a techno-economic analysis of a hydrogen-based system for an Italian city [18]. The presented system used excess electricity generated from wind turbines and PV panels to produce hydrogen, which was then combined with CO_2 to generate synthetic natural gas. The system's performance was evaluated using the levelized cost of synthesized natural gas, with two future scenarios for 2030 and 2050. Depending on investment costs and electricity prices, the levelized cost ranged from 70 to 325 €/MWh for 2030 and 37 to 233 €/MWh for 2050.

Pastore et al. assessed the economic potential of a residential Power-to-Gas hydrogen-based system [19]. In this case, hydrogen was blended into the natural gas network for sale. Utilizing Italy's self-consumption incentive of 170 €/MWh for PV self-consumed electricity, they found that levelized costs of hydrogen varied between 40 €/kgH2 and 0.96 €/kgH2 for 47.5 kW and 190 kW of PV, respectively. They compared this system to a battery-based Power-to-Power system, concluding that Power-to-Gas performs better under conditions of high PV overproduction.

Fonseca et al. studied a hydrogen-based system designed to meet residential electricity demand and supply hydrogen for 12 vehicles [20]. When insufficient energy was produced, electricity was drawn from the grid, and hydrogen was generated using natural gas. This system combined both Power-to-Power and Power-to-Gas applications. The system was optimized based on total annual cost, CO2 emissions, and grid dependence. Results showed a shift in design priorities depending on the objective: when optimizing for cost, hydrogen was primarily generated using natural gas, while in the emissions-optimized scenario, all hydrogen was produced via electrolysis.

From the literature alone, it is difficult to clearly identify which hydrogen application (Power-to-Power or Power-to-Gas) is best suited for residential settings. In the last two presented studies, both uses are explored. However, in Pastore et al. work only the Power-to-Gas system incorporates hydrogen components, while in Fonseca et al. study the two usages are combined in the same systems [19, 20]. A comparative study covering multiple hydrogen applications (Power-to-Power and Power-to-Gas) is therefore needed to clarify the optimal role of hydrogen-based systems in residential contexts. A summary of the studies in the literature can be found in Table 1.Another identified gap in the literature is that the life cycle environmental impacts of systems are rarely utilized for system sizing. While some studies estimate these indicators, they often do not incorporate them as objectives for optimization [3, 21]. As can be seen in Table 1 single-objective optimization studies typically focus on economic criteria, such as the total present system cost or energy cost. Occasionally, economic indicators may include environmental impacts by reintegrating externalities, such as carbon taxes and pollution costs [16]. Multi-objective optimization can combine economic criteria with technical or energy criteria (loss-of-load probability, production shortfalls, renewable energy usage, etc.), or with environmental criteria (greenhouse gas emissions, NOx emissions, land use, water consumption, etc.). However, in the cited studies, these impacts are generally considered only during the system's operational phase (emissions in operation, NOx generated, reduction in diesel used, etc.). This approach tends to favor large-scale systems without addressing the negative impacts these systems create during other phases of their life cycle (extraction of materials, assembly, transport, dismantling, etc.). Life cycle analysis accounts for these impacts, which penalizes oversized systems. Consequently, new and potentially more robust design trends can emerge when life cycle emissions are used as optimization objectives.

Furthermore, in all the studies presented in Table 1, building loads are treated solely as input data for the system model and remain decoupled from the operation of the energy system. Consequently, the

multi-energy system is assumed to have no influence on the thermal behavior of the building. Moreover, as shown in Table 1, most studies employ an hourly temporal resolution, while only two of the identified references use a finer time step. However, using excessively large time steps can reduce the accuracy of the results. Armstrong et al. demonstrated the impact of temporal resolution in a study of a cogeneration system supplying a residential building [23]. For the same building, the proportion of electricity exported increased from 24% with an hourly resolution to 30% with a 5-minute resolution. To address these two limitations identified in the literature, this study performs a system assessment based on a coupled building–energy system model and a temporal resolution of 1 minute. Combined with a life cycle assessment, these modeling improvements enable a more comprehensive evaluation of the performance of Power-to-Power and Power-to-Gas architectures.

A preliminary part of our work, which studied the impact of life cycle emissions on optimization results, has been published in a study on a Power-to-Power application in a British district [24]. The present study extends this publication by employing an improved version of the previously presented model to compare different applications (Power-to-Power and Power-to-Gas) of hydrogen-based multi-energy systems in residential settings. Given the gaps identified in the literature, this article aims to:

- Conduct a multi-objective optimization of residential hydrogen-based multi-energy systems using economic and energetic indicators, as well as whole life cycle greenhouse gas emissions.
- Assess and compare the performance of these systems across multiple architectures (Power-to-Power and Power-to-Gas).
- Identify the most pertinent applications of hydrogen-based systems in residential settings for various energy mixes.

The objective of this study is to address the following research questions:

- Is the use of hydrogen for supplying building energy demand (Power-to-Power) or for transportation applications (Power-to-Gas) the more cost-effective, environmentally sustainable, and energy-efficient pathway?
- At what electricity grid carbon intensity does a residential Power-to-Power hydrogen system become environmentally preferable to direct reliance on grid electricity?

Table 1 : Summary of hydrogen-based residential multi-energy systems in the literature

Reference	Time step	Scale	Hydrogen use	Evaluation criterion	Comment
Hosseini et al. (2013) [13]	1 h	1 building	Power-to-Power	Energetic	No optimization
Arsalis et al. (2018) [25]	1 h	1-100 habitations	Power-to-Power	Economic and environmental	No optimization
Gabrielli et al. (2018) [14]	1 h	24 buildings	Power-to-Power	Economic and environmental	
Samy et al. (2019) [26]	1 h	1 region	Power-to-Power	Economic and environmental	
Ghenai et al. (2020) [4]	30 min	1 Community	Power-to-Power	Economic	
Monforti Ferrario et al. (2021) [5]	1 h	1 building	Power-to-Power	Economic, technique and energetic	Cost, efficiency and safety
Fonseca et al. (2021) [20]	1 h	1 Community	Power-to-Power and Gas	Economic, technique and energetic	Cost, annual emissions and grid dependence
Mansir et al. (2022) [2]	1 h	1 building	Power-to-Power	Economic and environmental	
Babatunde et al. (2022) [6]	1 h	1 residence	Power-to-Power	Economic, environmental and technique	
Cikatić Šanić and Barbir (2022) [12]	1 h	1 house	Power-to-Power	Economic	
Fambri et al. (2022) [18]	1 h	1 city	Power-to-Gas	Economic	
Pastore et al. (2022) [19]	1 h	20 buildings	Power-to-Gas	Economic	Power-to-Power with battery
Mustafa et al. (2023) [16]	1 h	100 houses	Power-to-Power	Economic	Economic penalty for emissions
Kilic and Altun (2023) [7]	3 min	1 building	Power-to-Power	Economic and environmental	Hourly domestic load
Mohammed et al. (2023) [3]	1 h	1 laboratory	Power-to-Power	Economic and technique	Total cost and system reliability

Reference	Time step	Scale	Hydrogen use	Evaluation criterion	Comment
Ancona et al. (2023) [27]	1 h	1 building	Power-to-Power	Energetic	Optimization of the PV fraction used
Basnet et al. (2024) [22]	1 h	1 city	Power-to-Gas	Economic and environmental	Total cost and annual emission
Eldakadosi, and Schneeloch (2024) [17]	1h	13 houses	Power-to-Power	Economic and environmental	Emission in operation

2. Method

This section describes the methodological framework of the study, organized into three main components: the modeling of residential energy demand, the modeling of the multi-energy system and its operational strategy, and the optimization procedure used to evaluate system configurations over a representative annual simulation.

2.1. Residential load modeling

To evaluate system performance, residential electricity and heat demand must be accurately modeled. Demand profiles should be diverse to capture inter-household variability, coherent to represent load–generation mismatches, high-resolution to assess system dynamics, and continuous to evaluate storage potential.

These profiles are generated using a dedicated method fully described and validated in our previous work [31], where it was benchmarked against real-world residential measurement datasets. That study demonstrated the ability of the method to reproduce key statistical features of demand, including temporal variability, peak behavior, and household diversity. The same methodology is also used to generate PV production profiles in the present work.

These profiles are generated using a dedicated method, fully described in [28], which is also used to generate PV production profiles.

For electrical demand, behavioral patterns are generated stochastically, accounting for occupancy, appliance usage, lighting, and heating/cooling preferences. Combined with appliance and lighting characteristics, this approach produces stochastic electricity load profiles.

Thermal demand is modeled using a reduced-order RC network, enabling simulation of building thermal behavior at 1-minute resolution. The resulting indoor temperature evolution determines the electricity consumption of heating and cooling systems via a heat pump with a coefficient of performance (COP) of 2.57 at 0 °C. This gray-box model ensures low computational cost, allowing coupling with multi-energy system simulations and analysis of system impacts on building thermal behavior.

In this study, system performance is assessed for an energy-efficient district of 100 low-consumption houses located in Belfort, France. Building thermal properties are based on a Passive House–certified dwelling (Passivhaus Institute), which results in an atypical but physically consistent low-energy demand context. Average annual district energy consumption is reported in Table 2.

Table 2 : Average annual electricity consumption per home in the passive French neighborhood

Usage	Consumption
Electrical appliances	1661 kWh/year
Kitchen equipment	353 kWh/year
Lighting	221 kWh/year
Hot water	533 kWh/year
Space heating	782 kWh/year
Cooling	7 kWh/year
Total	3557 kWh/year

2.2. Multi-energy system modeling and operational strategies

This section presents the modeling framework adopted for the multi-energy system, covering the system architecture, the component-level models, and the strategy governing energy flows among subsystems. These elements together define how the hydrogen-based multi-energy system is represented and operated throughout the study.

2.2.1. Architecture

As previously noted, hydrogen-based multi-energy systems can be implemented at multiple scales and for different applications.

2.2.1.1. Power-to-Power architecture

In a Power-to-Power configuration, the system includes two energy storage subsystems: a battery subsystem, consisting only of batteries, and a hydrogen subsystem, which comprises an electrolyzer, hydrogen tank, fuel cell, and auxiliary components (e.g., power converters, heat exchangers, and purifiers).

The system collectively stores and distributes energy generated by all photovoltaic (PV) panels and interacts with both the residential loads and the PV systems installed on the buildings. Because the system is located remotely from individual dwellings, electricity and heat must be transmitted through dedicated distribution networks (Figure 1a).

2.2.1.1. Power-to-Gas architecture

In a Power-to-Gas configuration, hydrogen produced by the electrolyzer is not converted back into electricity but stored for sale. PV production continues to supply residential electrical demand, while all surplus electricity is diverted to hydrogen production. In time of low PV production the buildings heating is provided by heats pump alimented by the electricity grid.

As opposed to the Power-to-Power case, the goal of the system is here only to use the excess energy and not to produce power. As a result, the system does not include power generation components (Figure 1b) such as a fuel cell or a batterie. The hydrogen is then compressed and stored, with the tank

assumed to be emptied daily by early morning. Which correspond to suppose that the produced hydrogen is sold or used daily.

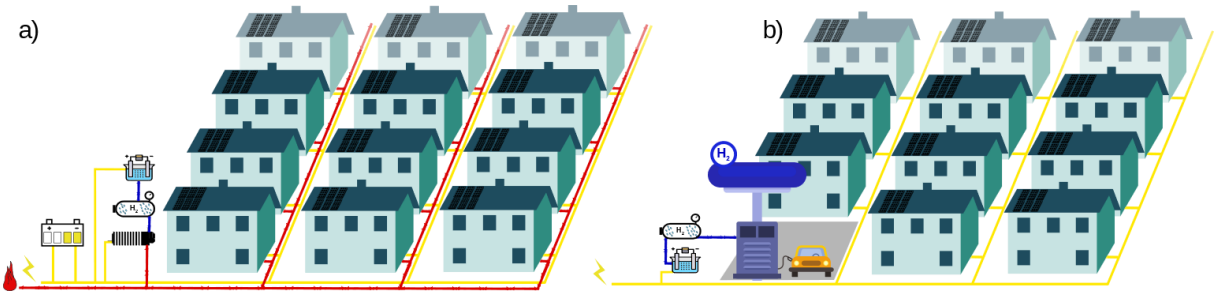

Figure 1 : Systems architectures, a) Power-to-Power b) Power-to-gas

2.2.2. Multi-energy components models

The models are based on global system efficiencies, which aggregate internal losses and auxiliary power consumption into single parameters.

2.2.2.1. Hydrogen components

The electrolyzer consumes electricity to convert water into hydrogen. The adopted model is derived from Ghenai et al. [4]. For a given power input, the corresponding hydrogen mass flow rate is calculated using the higher heating value (HHV) and the electrolyzer's efficiency (Eq. (1)), which varies with load factor according to Yue et al. [29].

$$\dot{m}_{H_2,pd} = \frac{\eta_{EC}.P_{EC}}{HHV_{H_2}} \quad (1)$$

The electrolyzer produces hydrogen at 50 bar. In Power-to-Gas applications, additional compression up to 700 bar is required. The associated energy consumption is calculated using a two-stage compression model with intercooling, following Khan et al. [30] (Eq. (2)). The compressor present, to consider non-ideality, an isentropic efficiency of 0.65 and a motor efficiency of 0.95, consistent with Parks et al. [31]. The hydrogen compressibility factor Z is set to 1.23, calculated using the CoolProp Excel plug-in [32].

$$P_{cp} = \frac{W_{is}}{\eta_{is}\eta_{mt}} * \frac{\dot{m}_{H_2}}{M_{H_2}} \quad (2)$$

With:

$$W_{is} = N * T_{in} * Z * R * \frac{\gamma}{\gamma - 1}\left(\left(\frac{Pr_{out}}{Pr_{in}}\right)^{\frac{\gamma-1}{N\times\gamma}} - 1\right) \quad (3)$$

Fuel cells convert stored hydrogen into electricity and heat. Their modeling follows an approach similar to Ranjbar and Kouhi [33]. For a given electrical demand, the hydrogen consumption is calculated using systems efficiencies, as described in Eq. (4). The corresponding thermal production is then calculated with Eq. (5).

$$\dot{m}_{H_2,cs} = \frac{P_{el,FC}}{HHV_{H_2} * \eta_{el,FC}} \quad (4)$$

$$P_{th,FC} = HHV_{H_2} * \eta_{th,FC} * \dot{m}_{H_2,cs} \quad (5)$$

For a district-scale system, constant efficiencies are assumed: 42.2% electrical and 33.8% thermal [34].

Operational constraints are imposed on hydrogen components to represent realistic system dynamics. Both the electrolyzer and the fuel cell operate within predefined load ranges, and their transient behavior is modeled using four operating phases: start-up, operation, standby, and shutdown, introducing delays before reaching nominal performance.

2.2.2.2. Battery

The battery stores and supplies electricity, leveraging its fast response and load flexibility to help balance the system. The model follows Ghenai and Bettayeb [35]. The battery's state of charge (SOC) is calculated at each time step based on the previous SOC and the energy charged or discharged during that period (Eq. (6)). To prolong the battery's lifespan, discharge is limited to a predefined depth of discharge (DOD) (Eq. (7)). Additionally, the battery's maximum charge and discharge power are constrained (Eq. (8) and (9)).

$$SOC(t) = \mathrm{SOC(t} - \Delta\mathrm{t)} + \frac{\eta_{ch} * P_{ba,ch} * \Delta t}{Q_{ba}} - \frac{P_{ba,di} * \Delta t}{\eta_{di} * Q_{ba}} \quad (6)$$

$$\begin{cases} SOC_{min} \leq SOC \leq 1 \\ SOC_{min} = (1 - DOD) \end{cases} \quad (7)$$

$$0 \leq P_{ba,ch} \leq P_{ba,max} \quad (8)$$

$$0 \leq P_{ba,di} \leq P_{ba,max} \quad (9)$$

Model parameters are taken from the literature (Table 3). Five values are not specified in the table, as they represent the optimization variables: PV size per house, nominal power of the fuel cells and electrolyzer, and the storage capacities of the battery and hydrogen tank.

Table 3 : multi-energy system parameters

Parameter	**Value**	**Reference**
PV area	**To optimize**	
PV nominal efficiency	16.9%	[13]
PV slop	40°	

PV direction	South	
PV efficiency temperature coefficient	-0.38%/°C	[13]
Electrolyzer nominal power	**To optimize**	
Electrolyzer efficiency	65–75%	[29]
Electrolyzer load range	25–100%	
Electrolyzer start-up delay	30 minutes	
Electrolyzer shutdown delay	11 minutes	
Compression stage	2	
Compression isentropic efficiency	65% (Power-to-Gas)	[31]
Compression motor efficiency	95% (Power-to-Gas)	[31]
Fuel cells nominal power	**To optimize**	
Fuel cells electric efficiency	42.2%	[34]
Fuel cells thermal efficiency	33.8%	[34]
Fuel cells load range (electric)	35–100%	[34]
Fuel cells start-up delay	5 minutes	
Fuel cells shutdown delay	0 minutes	
Hydrogen tank capacity	**To optimize**	
Battery capacity	**To optimize**	
Battery Depth of Discharge	80%	[36]
Battery max charging rate	1C	
Battery max discharging rate	1C	
Battery charge efficiency	92%	[36]
Battery discharge efficiency	92%	[36]
DC/DC converter efficiency	95%	[37]
DC/AC converter efficiency	95%	[37]
Heat transfer efficiency	78%	[38]

2.2.3. Energy flow distribution strategy

At the component level, the system follows a rule-based strategy to determine which component absorbs or supplies energy at each time step. The Power-to-Power strategy is described in detail in previous works [24]. The energy management strategy adopted in this study is rule-based. This choice

was made to maintain consistency with control approaches that remain widely used in current district heating applications and to isolate the effect of component sizing and architecture choices from that of advanced operational optimization.

At the system level, buildings prioritize self-consumption: PV energy first meets local demand, while overproduction or unmet demand is managed by the multi-energy system. Component availability is checked sequentially, with priority given to the battery. If a single component cannot fully absorb or supply the required power, other components assist. Any residual deficit is supplied by the grid, and any excess energy is fed back into the grid.

The system also adjusts operations to mitigate hydrogen system dynamics. When the battery is nearly full (>85% SOC), half of the electricity is diverted to the electrolyzer to smooth start-up. Similarly, the fuel cell remains active until the battery reaches >80% SOC to reduce frequent ON/OFF cycles.

With specified component sizes (PV panels, battery, electrolyzer, fuel cell, and hydrogen tank), the system's annual behavior can be simulated. An example simulation for 1960 m² PV, 650 kWh battery, 36.2 kW electrolyzer, 17.6 kW fuel cell, and 492 kg H_2 tank is shown in Figure 2.

In the Power-to-Gas scenario, the system absorbs only excess PV energy via hydrogen production, while maintaining self-consumption priority. The electrolyzer is activated only when PV generation exceeds demand and the hydrogen tank is not full. The exception occurs if the electrolyzer is already running and PV generation drops below its minimum output; in such cases, the grid supplies up to 75% of the required power, avoiding frequent ON/OFF cycling.

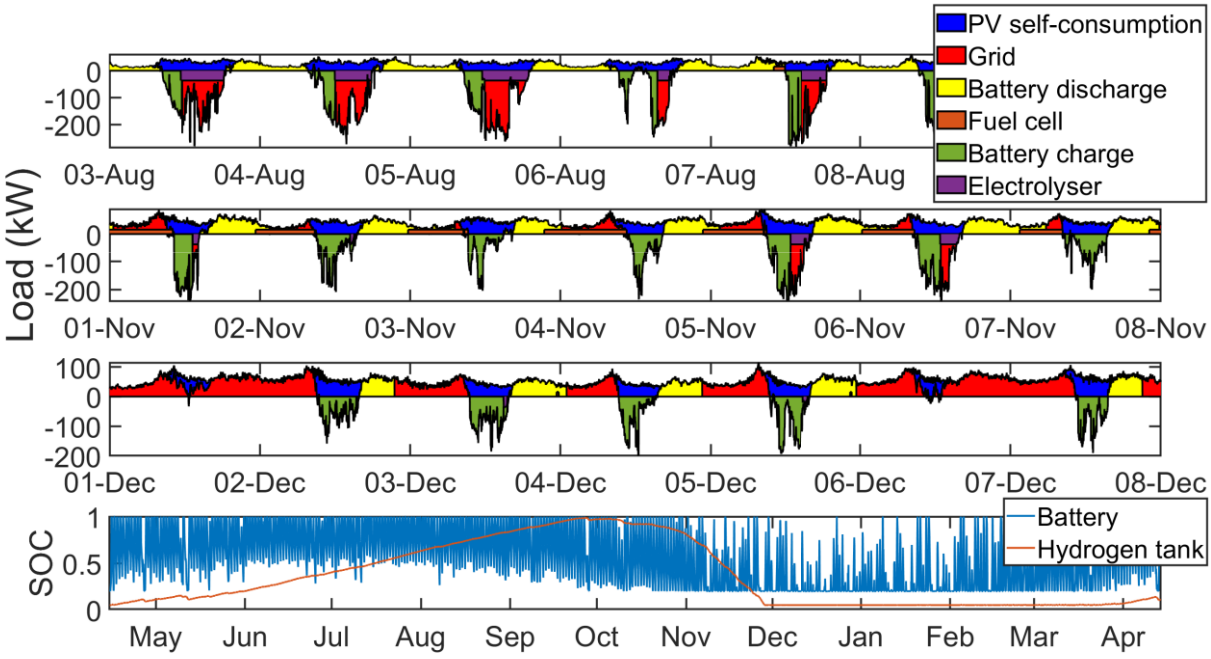

Figure 2 : Multi-energy system yearly behavior for a Power-to-Power application at district scale

2.3. Optimization

For a given component configuration, the system is simulated over a full year, starting on April 15, considered the end of the heating season, when the hydrogen reservoir is assumed empty (no inter-annual storage is considered). System performance is then assessed based on the evolution of buildings and components throughout the year, following the methodologies described in the previous sections.

2.3.1. Objective functions

The optimization considers three objective functions, each capturing a distinct dimension of system performance: energetic, economic, and environmental. These objectives are evaluated to characterize the trade-offs associated with different component configurations.

2.3.1.1. Renewable Energy Proportion

The first step is to evaluate the energy supplied to the buildings. Heat and electricity balances are computed for all buildings at each time step. For thermal demand, the energy balance accounts for domestic hot water (DHW) and space heating (Eq. (10)). If the rest is positive, all the power supplied is useful (positive part of Eq. (11)). If production exceeds demand, only the energy meeting the load plus the amount that can be stored in the DHW tank is useful (negative part of Eq. (11)). Finally, the energy provided is adjusted by the heating system efficiency to estimate the actual energy provided (Eq. (12)).

$$P_{re,th} = P_{DHW} + P_{he} - P_{FC,th} \quad (10)$$

$$P_{rt,th} \begin{cases} \geq 0 \rightarrow P_{pr,th} = P_{FC,th} \\ < 0 \rightarrow P_{pr,th} = P_{DHW} + P_{he} + P_{ab} \end{cases} \quad (11)$$

$$E_{pr,th}(t) = \frac{(P_{pr,th}) * \Delta t}{COP} \quad (12)$$

For electricity, the building demand is compared with component generation to determine the electrical deficit (Eq. (13)). If the system cannot fully meet demand, the grid supplies the remainder (positive part of Eq. (14)). Conversely, if production exceeds demand and storage capacity, excess electricity is considered rejected, and the grid contribution is zero (negative part of Eq. (14)). The electricity directly supplied by the system is then calculated as the building demand minus the grid supply (Eq. (15)).

$$P_{rt,el} = P_{dm,el} + P_{ba,ch} + P_{EC} - P_{PV} - P_{FC,el} - P_{ba,di} \quad (13)$$

$$P_{rt,el} \begin{cases} > 0 \rightarrow P_{gr,el} = P_{rt,el} \\ < 0 \rightarrow P_{gr,el} = 0 \end{cases} \quad (14)$$

$$E_{pr,el}(t) = (P_{dm,el} - P_{gr,el}) * \Delta t \quad (15)$$

The energy supplied is subsequently used to assess system performance, either through energy savings for buildings (section 2.3.1.2) or mitigated greenhouse gas emissions (section **Erreur ! Source du renvoi introuvable.**). It also enables calculation of energy indicators, such as local production or PV utilization. The primary indicator in this study is the Renewable Energy Proportion (REP), defined as the ratio of energy from renewable sources to total system consumption (Eq. (16)). Energy from renewables includes the thermal and electrical energy supplied by the system, plus the grid-supplied electricity adjusted for the French grid's renewable fraction (data from [39]).

$$Ob_{REP} = max(REP) = max\left(\frac{\sum_t \left[E_{pr,el}(t) + E_{pr,th}(t) + E_{gr}(t) \times fr_{gr}(t)\right]}{\sum_t E_{dm,tt}(t)}\right) \quad (16)$$

2.3.1.2. Net Present Cost

For economic assessment, the total net present cost (NPC) of the system is used as the objective function. System costs are divided into four categories, (Eq. (21)): initial investment (Eq. (17)), component replacement (Eq. (18)), operation and maintenance (Eq. (19)) and electricity purchase if needed (Eq. (20)). The discount factor is calculated using a nominal discount rate of 0.09 and an inflation rate of 0.014 [40].

Initial investment costs are based on component size (Table 4), with calculation methods varying by component. Following the literature, only fuel cells and batteries are replaced after 10 years, and operation-induced degradation is neglected [41, 36]. Operation and maintenance costs are set at 3% of initial investment for all components except the battery, consistent with Gracia et al. [36]. Electricity purchase costs are based on hourly market prices for 2023 [42].

Economic gains are then estimated by quantifying the electricity and heat supplied to buildings over the simulated year (Section 2.3.1.1). Energy supplied is converted into economic value using hourly electricity tariffs for French households [43] (Eq. (24)). For Power-to-Gas applications, revenues from hydrogen production are also included (Eq. (25)). Combining costs and gains, the NPC is calculated (Eq. (26)), with all parameters summarized in Table 5. With this formulation, a system configuration is considered competitive with grid reliance when its NPC is negative.

$$C_{iv} = \sum_{j \in sys} \left[C_j(S_j)\right] \quad (17)$$

$$C_{rm} = \sum_{j \in csys} \left[C_j(S_j) \times \sum_{y \in y_{rm}} \left[\frac{1}{(1 + tx_{dc,r})^y}\right]\right] \quad (18)$$

$$C_{O\&M} = \frac{1}{CRF} \sum_{i \in sys} \left[C_i(S_i) \times tx_{O\&M,i}\right] \quad (19)$$

$$C_{by} = \frac{1}{CRF} \times \sum_{t \epsilon y} \left[Eng_{by}(t) \times C_e(t)\right] \quad (20)$$

$$C_{tt} = C_{iv} + C_{rm} + C_{O\&M} + C_{by} \quad (21)$$

With :

$$tx_{dc,r} = \frac{tx_{dc,nm} - tx_{if}}{1 + tx_{if}} \quad (22)$$

$$CRF = \frac{tx_{disc,r} \times \left(1 + tx_{dc,r}\right)^{lt}}{\left(1 + tx_{dc,r}\right)^{lt} - 1} \quad (23)$$

$$G = \frac{1}{CRF} \sum_{t \epsilon year} \left[Eng_{pr}(t) \times C_{el}(t)\right] \quad (24)$$

$$G_{sl,H2} = \frac{1}{CRF} \times m_{H2,sl} \times C_{H2} \quad (25)$$

$$Ob_{eco} = min(NPC) = min(C_{tt} - G - G_{sl,H2}) \quad (26)$$

Table 4 : investment cost calculation

Components	**a**	**b**	**Transition**	**Formula**
PV panels [36]	1670 €/kWp			$C = a \times S$
Battery [36]	550 €/kWh			$C = a \times S$
Electrolyzer [14]	{2693;1727;1354} €/kW	{0;193200;491600} €	{200;800} kW	$C = a_n \times S + b_n$
Fuel cell [14]	{2160;1680;1320} €/kW	{0;384000;960000} €	{800;1600} kW	$C = a_n \times S + b_n$
Hydrogen tank [14]	{690;453;363} €/kg_{H2}	{0;355;15340} €	{1.5;166.5} kg	$C = a_n \times S + b_n$
Compressor [31]	9140 €.h/kg_{H2}	0.8		$C = a \times S^b$

Table 5 : Cost optimization parameters

System	**Investment**	**Lifetime**	**O&M (per year)**	**Ref.**
PV (monocrystalline)	1670 €/kWp	20 years	3% investment	[36]
Battery (Li-ion)	550 €/kWh	10 years	0% investment	[36]
Electrolyzer (PEM)	Cf. Table 4	20 years	3% investment	[36]
Fuel cells (PEM)	Cf. Table 4	10 years	3% investment	[41, 36]
Hydrogen tank	Cf. Table 4	20 years	3% investment	[36]
Compressor	Cf. Table 4	20 years	3% investment	[36]
Domestic electricity cost	0.17 €/kWh[a]			[43]
Market electricity cost	97 €/MWh[a]			[42]

a: annual mean of the hourly profiles

2.3.1.3. Life Cycle Emission

The environmental analysis uses a life-cycle-based indicator: the system's equivalent CO_2 emissions, which quantify its global warming potential. Component Life Cycle Assessment (LCA) are taken from the literature.

The methodology mirrors the cost analysis, summing the emissions of all components to estimate the system's life cycle emissions. Emissions do not scale linearly with size; the approach of Bahlawan et al. [44] is applied to extrapolate from a reference size (Eq. (27)), with a scaling factor (L) of 0.8 for most

components, based on Gabrielli et al. [14]. For PV panels, emissions scale linearly due to modular distribution across dwellings. For the hydrogen compressor, the scaling factor is adjusted using Vincent Knop's data [45]. All parameters are summarized in Table 6. Life cycle emissions are computed by aggregating component CO_2 equivalents (Eq. (28)). Emissions from purchased electricity are included using the same carbon intensity profile. The life-cycle emission factors used for each component exclude emissions reduction through recycling. Details on the methodology can be found in the references specified in Table 6.

Energy savings are expressed as emissions avoided from energy supplied (Eq. (29)), calculated using the hourly carbon intensity of the French electricity grid for 2021 [39]. In Power-to-Gas applications, avoided emissions from hydrogen production are also included (Eq. (30)). The system's overall greenhouse gas performance is then evaluated as the difference between its life cycle emissions and the emissions avoided during operation (Eq. (31)). With this formulation, a system configuration is considered competitive with grid reliance when its LCA emissions are negative.

$$\mathrm{Em} = \mathrm{Em}_{rf}\left(\frac{S}{S_{rf}}\right)^{L} \tag{27}$$

$$Em_{sys} = \sum_{i \in sys}\left[Em_{i,it}(S_i) + Em_{i,rm}(S_i)\right] + \sum_{t \epsilon y}\left[E_{by}(t) \times Em_e(t)\right] \tag{28}$$

$$Em_{av} = lifetime * \sum_{t \epsilon y}\left[E_{pr}(t) \times Em_{el}(t)\right] \tag{29}$$

$$Em_{sl,H2} = m_{H2,sl} \times Em_{H2} \tag{30}$$

$$Ob_{en} = min(Em_{LCA}) = min(Em_{sys} - Em_{av} - Em_{sl,H2}) \tag{31}$$

Table 6 : parameters for components life cycle emissions calculation

Composants	**S_{rf}**	**Em_{rf} ($kgCo_2eq$)**	**L**
PV panels [46]	1 kWc	2113 $kgCo_2eq$	1
Battery [47]	550 kWh	71885 $kgCo_2eq$	0.8
Electrolyzer [48]	998 kW	29341 $kgCo_2eq$	0.8
Fuel cell [49]	80 kW	2400 $kgCo_2eq$	0.8
Hydrogen tank [49]	5.5 kg	1590 $kgCo_2eq$	0.8
Compressor [45]	1 kg/h	7238 $kgCo_2eq$	0.67

2.3.2. Multi-objective optimization technique

The model is applied within a simulation-based multi-objective optimization framework. In this approach, an optimization algorithm proposes values for the state variables, which the simulation evaluates to determine system performance. The algorithm then updates the variables for the next iteration. This process continues until convergence criteria are met.

Simulations cover a full year, starting on April 15. The five optimization variables are the sizes of the system components: fuel cell electrical power (FC), electrolyzer power (EC), hydrogen tank capacity, battery capacity (Bat), and PV panel surface area. Each configuration is evaluated using the three objective functions described previously.

Prior to multi-objective optimization, three single-objective optimizations are performed to identify the relative optima. Due to the high temporal resolution (1 min) and 1-year simulation horizon, evaluating the objective functions is computationally intensive: for a 100-home neighborhood, a single evaluation requires ~3 minutes on a 3.8 GHz processor. To reduce computational time, the MATLAB® surrogate optimization tool is employed, using a surrogate model to minimize the number of full evaluations.

The relative optima then serve as starting points for the MATLAB® multi-objective elitist genetic algorithm, which generates the Pareto front. To improve Pareto front coverage, nondominated points are extracted from all generations, not just the final one. Configurations that appear clearly non-optimal, such as those including only a single hydrogen component, are reevaluated to ensure accuracy.

3. Results and discussion

This section presents the results obtained for the two multi-energy system configurations introduced in the Method section: Power-to-Power and Power-to-Gas. For each configuration, system performance is analyzed according to the relevant economic, environmental, and energetic criteria, highlighting the trade-offs associated with component sizing and operational strategy.

3.1. Power-to-Power

In the Power-to-Power application, the system stores photovoltaic energy to meet electrical and thermal demands during periods of low solar irradiation. All five components are used: PV panels, battery, electrolyzer, fuel cell, and hydrogen tank. System performance is evaluated using economic, emission, and energy criteria. As described in Section 2.1, the system interacts with the energy demand of an energy-efficient district of 100 passive single-family houses in Belfort, France.

3.1.1. Base Case Study

The base case considers a district-scale system, with a single system serving all houses. Thermal output from the fuel cell is distributed via a district heat network. The Pareto front obtained from multi-objective optimization for the three objectives is shown in Figure 3. From this Pareto front, three configurations are selected using LINMAP, TOPSIS, and GRA. LINMAP identifies the alternative closest to an ideal point, TOPSIS ranks alternatives based on distance to ideal and anti-ideal solutions, and GRA evaluates alternatives using grey relational similarity under uncertainty [50].

The mono-objective optima and selected configuration sizes are summarized in in Table 7. The cost-optimal configuration consists solely of PV panels (2.2 m² per dwelling), increasing the renewable energy proportion in each house by 10%. The CO_2 emission optimum corresponds to no multi-energy system, yielding no economic or environmental gains. The renewable energy proportion optimum features larger components, capable of meeting the entire annual load via daily battery storage and seasonal hydrogen storage.

Among the Pareto-based selections, TOPSIS and LINMAP choose configurations with seasonal storage, but storage is limited to early winter. The GRA method selects a smaller system, with a limited PV area producing minimal overproduction, and hydrogen storage used only for daily cycling.

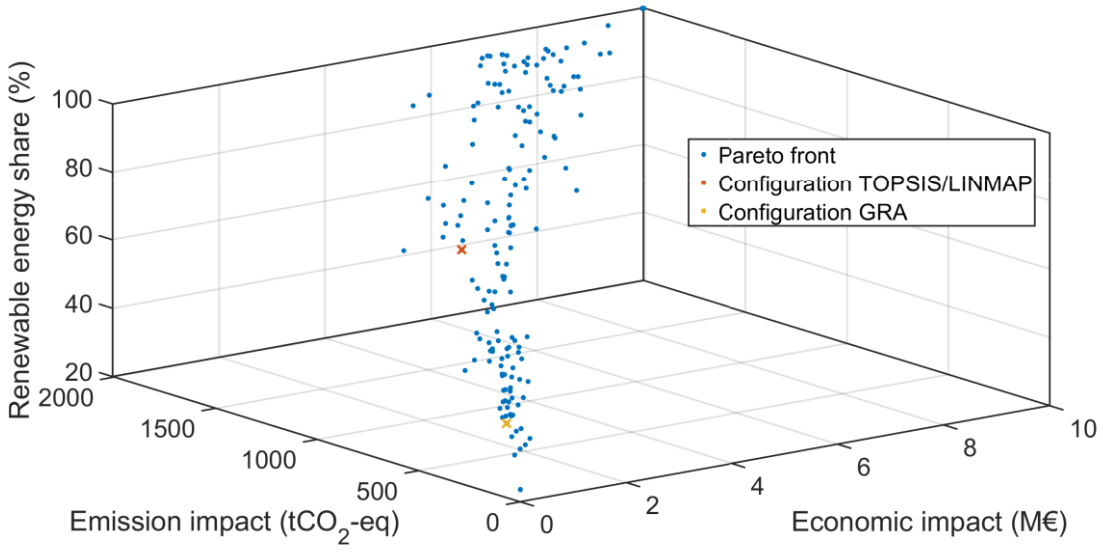

Figure 3 : Pareto front cost, emissions and renewable energy proportion (passive French case)

Table 7 : Sizes of mono-objective optimums and selected configurations (passive district French case)

Component	**Economic Optimum**	**Emission Optimum**	**GRA**	**TOPSIS et LINMAP**	**REP Optimum**
PV (monocrystalline)	220 m²	0 m²	465 m²	1959 m²	5000 m²
Battery (Li-ion)	0 kWh	0 kWh	23.4 kWh	651 kWh	436 kWh
Electrolyzer (PEM)	0 kW	0 kW	5.1 kW	36.2 kW	1 MW
Fuel cell (PEM)	0 kW	0 kW	0.35 kW	17.6 kW	600 kW
Hydrogen tank	0 kg_{H2}	0 kg_{H2}	4.6 kg_{H2}	492 kg_{H2}	7781 kgH2
NPC	-9.6 k€	0 k€	44.2 k€	1223 k€	9992 k€
LCA Emission	25.7 tCO_2eq	0 tCO_2eq	79 tCO_2eq	609 tCO_2eq	2008 tCO_2eq
REP	33.3 %	23.5 %	41.4 %	79.1 %	100 %

Achieving sufficient hydrogen storage to cover the entire heating season is crucial for maximizing renewable energy utilization. However, under the considered assumptions, hydrogen storage systems remain economically and environmentally uncompetitive with the electricity grid, resulting in a strong deterioration of the other two objectives. While the energy objective inherently favors oversized systems, more meaningful configurations emerge when this objective is balanced against system cost or life-cycle emissions.

3.1.2. Variation of Energy Mix

Section 3.2.1 identifies the low carbon intensity of the French electricity grid as a limiting factor for system performance. To further investigate this effect, system performance is evaluated under three alternative electricity mixes. Electricity prices are derived from Eurostat data [51], while hourly carbon

intensity and renewable shares are obtained from Electricity Map [39]. The selected mixes correspond to the United Kingdom, Germany, and Poland, with mean annual carbon intensities of 252, 438, and 857 gCO_2/kWh, respectively. For comparison, average 2023 grid carbon intensities are estimated at 545 gCO_2/kWh in Africa, 590 gCO_2/kWh in Asia, 344 gCO_2/kWh in North America, 259 gCO_2/kWh in Latin America, and 490 gCO_2/kWh in Oceania [52]. Only electricity grid parameters are modified, and results therefore do not represent an actual relocation of the system, but rather potential future evolutions of the French energy mix, such as nuclear phase-out or increased renewable penetration.

Multi-objective optimizations are conducted for each energy mix, yielding three additional Pareto fronts (Figure 4). From an economic perspective, differences between mixes with high renewable shares remain limited, due to relatively small variations in electricity tariffs. The higher electricity price in the German mix slightly favors the multi-energy system; however, this improvement remains insufficient to render most Pareto-optimal configurations economically competitive. More pronounced differences are observed for smaller system configurations (Table 8).

The renewable energy proportion achievable with economically neutral systems (net economic impact ≈ 0) vary strongly with the electricity mix. For the French and Polish mixes, similar system configurations and renewable proportion are obtained. In contrast, the British and German cases show a marked increase in renewable energy proportion, driven by the economic viability of larger multi-energy systems. These configurations are summarized in Table 9.

From an environmental–RES perspective, differences between energy mixes are more pronounced. The French mix is the only case where the no-system configuration (0 tCO_2eq impact) lies on the Pareto front, indicating that in all other mixes, the system simultaneously reduces emissions and increases renewable energy use. Emission-optimal configurations are reported in Table 10. In the British mix, the optimum achieves approximately 75% renewable energy proportion, whereas the Polish and German mixes approach 100%. In all cases, the optimal configuration combines PV and battery storage for daily balancing with hydrogen storage for seasonal demand.

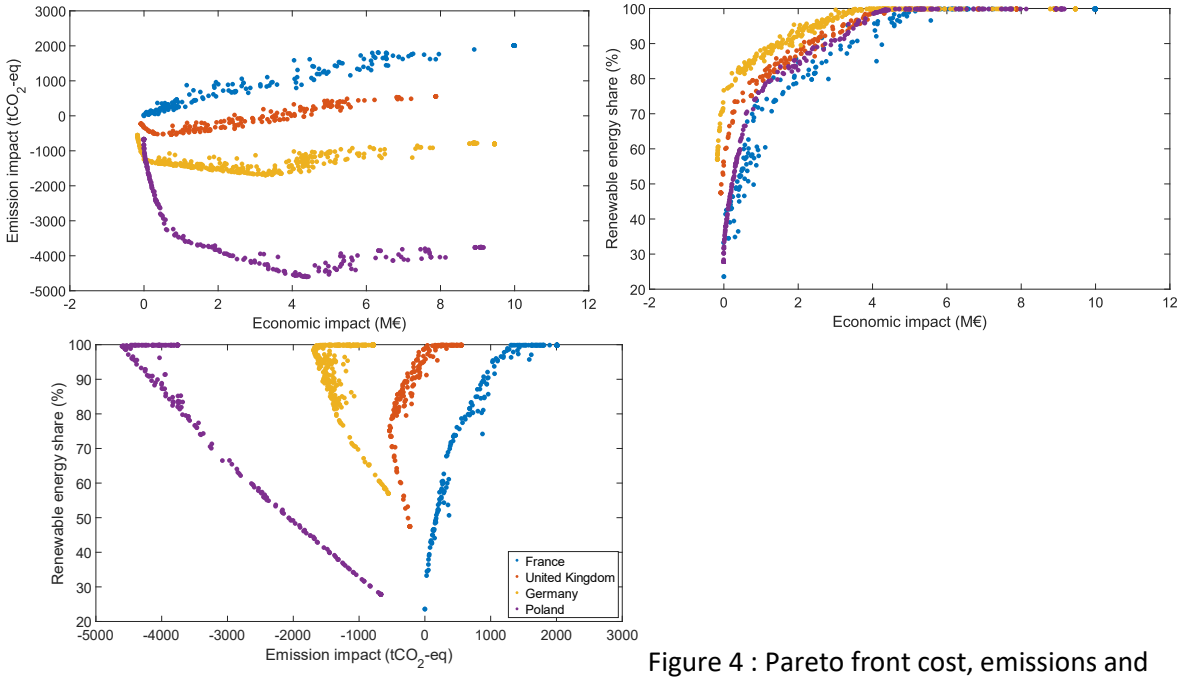

Figure 4 : Pareto front cost, emissions and renewable energy proportion for 4 energy mix

Table 8 : Economic optimum by energy mix

Component	**France**	**United Kingdom**	**Germany**	**Poland**
PV (monocrystalline)	220 m²	368 m²	528 m²	202 m²
Battery (Li-ion)	0 kWh	6.2 kWh	23.6 kWh	0 kWh
Electrolyzer (PEM)	0 kW	0 kW	0 kW	0 kW
Fuel cell (PEM)	0 kW	0 kW	0 kW	0 kW
Hydrogen tank	0 kgH2	0 kgH2	0 kgH2	0 kgH2
NPC	-9.6 k€	-81 k€	-176 k€	-6 k€
LCA Emission	25.7 tCO_2eq	-229 tCO_2eq	-554 tCO_2eq	-671 tCO_2eq
REP	33.3 %	47.4 %	57 %	27.9 %

Table 9 : Cost-effective configurations with the highest REP by energy mix

Component	France	United Kingdom	Germany	Poland
PV (monocrystalline)	220 m²	741 m²	1448 m²	302 m²
Battery (Li-ion)	0 kWh	82.5 kWh	458 kWh	0 kWh
Electrolyzer (PEM)	0 kW	4.2 kW	1.6 kW	0 kW
Fuel cell (PEM)	0 kW	0.3 kW	0.3 kW	0 kW
Hydrogen tank	0 kg_{H2}	3.8 kg_{H2}	2.9 kg_{H2}	0 kg_{H2}
NPC	-9.6 k€	-8.5 k€	-2.8 k€	-0.3 k€
LCA Emission	25.7 tCO_2eq	-321 tCO_2eq	-1244 tCO_2eq	-925 tCO_2eq
REP	33.3 %	56.3 %	76.7 %	31.7 %

Table 10 : Emission optimum by energy mix

Component	France	United Kingdom	Germany	Poland
PV (monocrystalline)	0 m²	1249 m²	2655 m²	2776 m²
Battery (Li-ion)	0 kWh	490 kWh	952 kWh	1.1 MWh
Electrolyzer (PEM)	0 kW	131 kW	336 kW	333 kW
Fuel cell (PEM)	0 kW	18 kW	53 kW	64 kW
Hydrogen tank	0 kg_{H2}	31 kg_{H2}	3.7 t_{H2}	3.9 t_{H2}
NPC	0 k€	737 k€	3.3 M€	4.4 M€
LCA Emission	0 tCO_2eq	-538 tCO_2eq	-1688 tCO_2eq	-4601 tCO_2eq
REP	23.5 %	75.1 %	98.4 %	99.6 %

To extend the analysis to all European Union electricity mixes, the emission-optimal configuration identified for the British case (Table 10) is evaluated across Europe. This configuration is hereafter referred to as OPT_EM_UK. Performance indicators are recalculated using country-specific electricity prices from Eurostat [51], and annual grid carbon intensity and renewable energy proportion data from Electricity Map [39]. The corresponding input data are summarized in Appendix A. Using annual averages instead of hourly profiles introduces approximation errors. For the four previously analyzed mixes, these errors range from 5–9% for emission reductions and 1–4% for renewable energy proportion estimates.

From an economic perspective, the results are shown in Figure 5. OPT_EM_UK does not generate a positive net present cost over 20 years for any European electricity mix, although economic impacts vary widely. In the most favorable case (Netherlands, 0.475 €/kWh), the system reaches a net present

cost of 341 k€, while in the least favorable case (Bulgaria, 0.114 €/kWh), the cost increases to 1.15 M€ over 20 years.

Emission performance is presented in Figure 6. For most EU countries, the configuration achieves 20-year emission reductions between 1,500 tCO_2eq and carbon neutrality. OPT_EM_UK reaches carbon neutrality or net-negative emissions in all countries except France and Sweden, whose grids are already highly decarbonized (52 and 28 gCO_2eq/kWh, respectively).

The renewable energy proportion achieved by OPT_EM_UK ranges from 70% to 90%, indicating that in grids with high renewable penetration, the system nearly eliminates reliance on non-renewable sources. Renewable Proportion close to 90% are observed in Sweden, Austria, and Denmark, whose electricity mixes are dominated by renewables. Countries in the upper-right quadrant of Figure 8 exhibit the highest renewable shares, while those in the lower-right quadrant rely more heavily on nuclear power. Fossil fuel–dominated systems are primarily located in the lower-left quadrant.

Across all investigated scenarios, several conclusions remain robust. In a Power-to-Power configuration, multi-energy systems are not economically competitive with the electricity grid without dedicated financial incentives. Nevertheless, in all cases, the systems substantially increase the share of renewable energy used by residential buildings. From an emissions perspective, while such systems do not outperform highly decarbonized grids (e.g., France), they achieve significant emission reductions in most European electricity mixes.

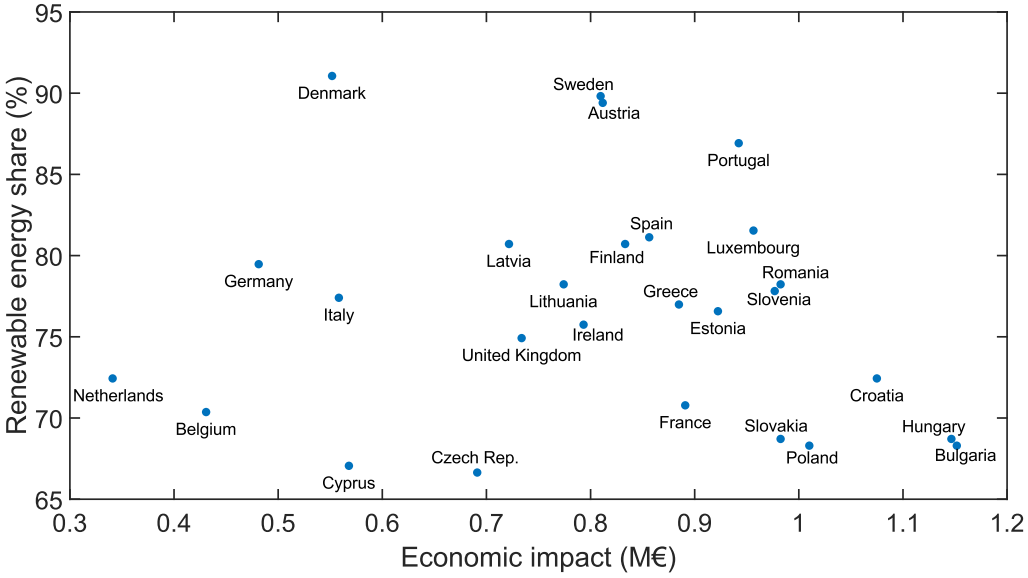

Figure 5 : Evolution of economic and renewable energy performances of selected configuration (OPT_EM_UK)

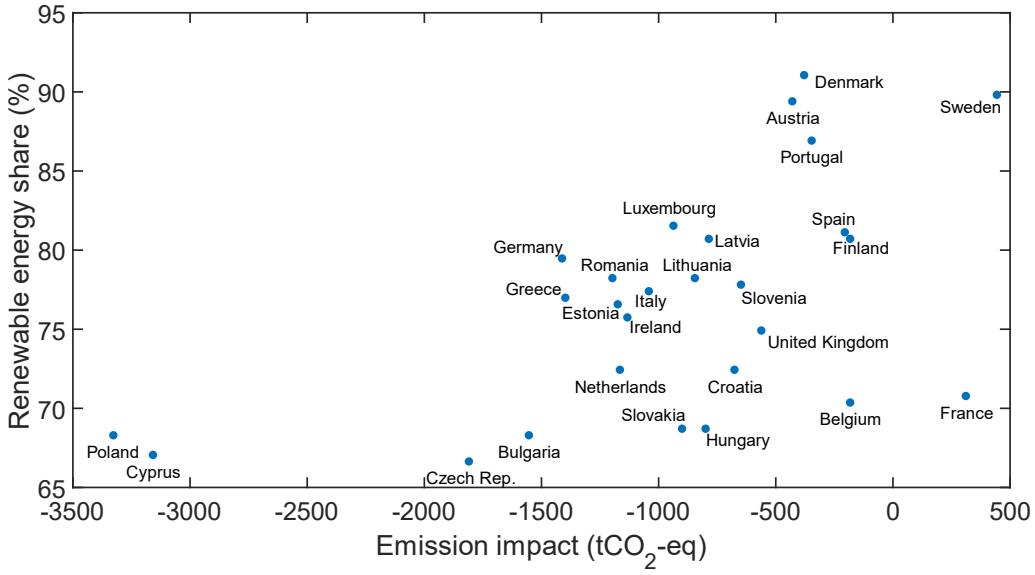

Figure 6 : Evolution of emission and renewable energy performances of selected configuration (OPT_EM_UK)

3.1.3. Component-level cost and emission reduction requirements

Beyond the influence of grid parameters, the techno-economic and environmental performance of the multi-energy system is strongly determined by the contribution of its individual components (PV array, electrolyzer, fuel cell, hydrogen tank, and battery). To quantify this contribution, three representative configurations were extracted from the Pareto front of the French case study, corresponding to REP of approximately 99%, 75%, and 50% (denoted FR-99-ENR, FR-75-ENR, and FR-50-ENR, respectively). Component sizing and their respective shares of system cost and emissions for each configuration are reported in Table 11.

For the FR-99-ENR configuration, the system shows an overall economic impact of approximately €5M over its 20-year lifetime, with component-related costs reaching €5.6M, dominated by the hydrogen tank (Table 11). Self-generated energy offsets €641k, but this remains insufficient to achieve competitiveness, requiring a component cost reduction of nearly 90%. As REF decreases, the system scales down and the required cost reduction generally diminishes: FR-75-ENR, where PV and the electrolyzer are the dominant cost contributors (Table 11), requires a 75% reduction, while the more compact FR-50-ENR configuration shows only €800k in net economic impact yet paradoxically demands an 80% reduction. For each configuration on the Pareto front of the French case study, the cost reductions required to achieve economic competitiveness with the grid are reported in Figure 7. For most configurations, the required reductions lie between 60% and 90%.

A parallel analysis was conducted for the environmental indicator. For FR-99-ENR, the lifecycle impact amounts to 1255 tCO_2eq, with component-related emissions of 1726 tCO_2eq, attributable mainly to the PV array (Table 11). The 470 tCO_2eq credit from system-generated renewable energy is again insufficient to reach carbon neutrality, necessitating a 73.4% reduction in component emissions. For FR-75-ENR, the required reduction drops to 64.2%, corresponding to specific reductions of PV emissions from 2113 to 756 $kgCO_2eq \cdot kWp^{-1}$, battery emissions from 144 to 51.6 $kgCO_2eq \cdot kWh^{-1}$, and hydrogen tank emissions from 113 to 40.5 $kgCO_2eq \cdot kgH_2^{-1}$ (Table 11). Notably, extending battery service life from 10 to 20 years alone would yield a 50% reduction in its associated lifetime emissions.

For FR-50-ENR, where component impact is almost entirely attributable to PV and the battery (Table 10), a 54% reduction is required (PV: 2113 to 972 $kgCO_2eq \cdot kWp^{-1}$; battery: 182 to 83.6 $kgCO_2eq \cdot kWh^{-1}$). For each configuration on the Pareto front of the French case study, the emission reductions required to achieve carbon neutrality with the grid are reported in Figure 8. Overall, the required reductions are smaller than those for the economic indicator, but in most cases remain above 50%.

Overall, the improvements in life-cycle costs and emissions needed to make the multi-energy system competitive with the electric grid are significant, and become even more significant as the desired share of renewable energy increases. Whether from an economic or environmental perspective, reducing the impact of the components alone does not seem realistic as a means of making the system competitive.

Table 11 : Share of costs and emissions for each component in 3 configurations

Component	Size	Share of cost	Share of emission
FR-99-ENR			
PV (monocrystalline)	3283 m²	21.6 %	67.9 %
Battery (Li-ion)	977 kWh	14.2 %	13.2 %
Electrolyzer (PEM)	491 kW	24.2 %	1 %
Fuel cell (PEM)	98 kW	6.8 %	0.3 %
Hydrogen tank	3.9 t_{H2}	33.3 %	17.6 %
FR-75-ENR			
PV (monocrystalline)	1805 m²	32.7 %	78.7 %
Battery (Li-ion)	336 kWh	13.5 %	11.8 %
Electrolyzer (PEM)	212 kW	36 %	1 %
Fuel cell (PEM)	15 kW	2.8 %	0.2 %
Hydrogen tank	598 kgH2	14.9 %	8.3 %
FR-50-ENR			
PV (monocrystalline)	723 m²	25.6 %	81.1 %
Battery (Li-ion)	106 kWh	8.3 %	12.1 %
Electrolyzer (PEM)	42 kW	14.3 %	0.7 %
Fuel cell (PEM)	128 kW	47.8 %	2.2 %
Hydrogen tank	70 kg_{H2}	4 %	3.8 %

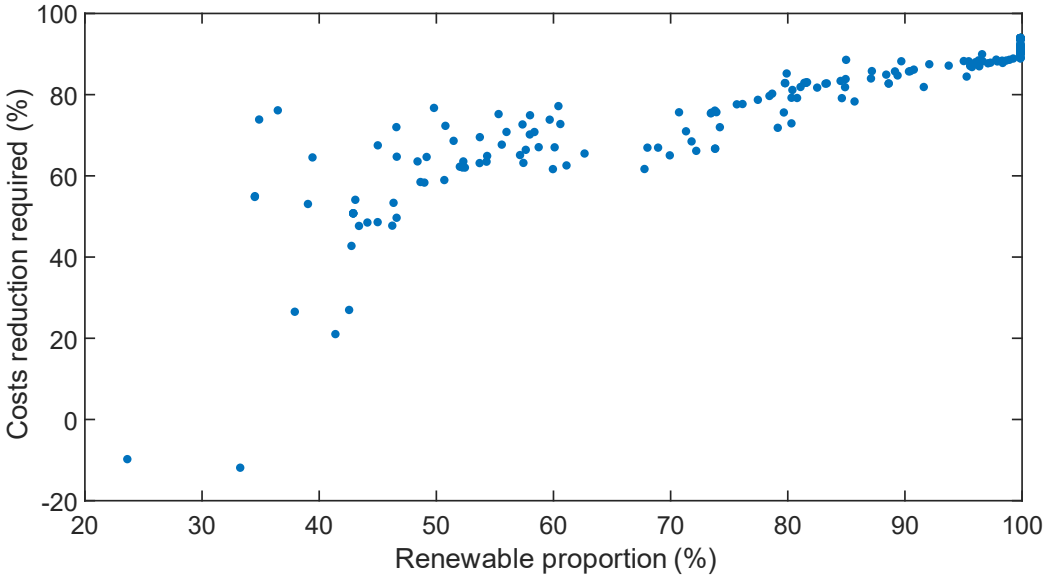

Figure 7 : System cost reductions needed to make it competitive with the grid

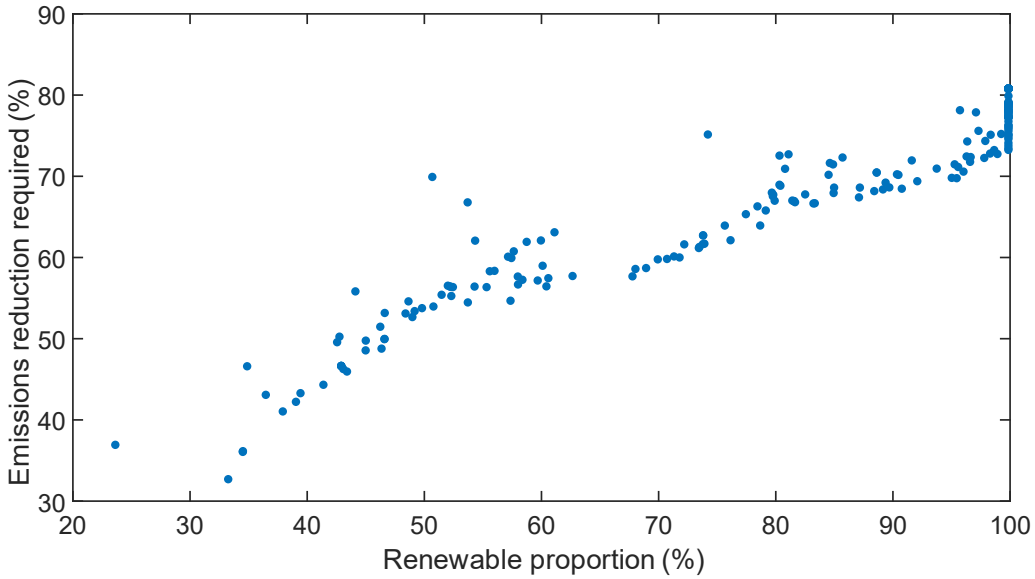

Figure 8 : System emission reductions needed to make it competitive with the grid

3.2. Power-to-Gas

In the Power-to-Gas configuration, photovoltaic overproduction is not stored to meet local demand, but converted into hydrogen for external use. This application relies on three components only: photovoltaic panels, an electrolyzer, and a hydrogen tank. System performance is assessed using economic and environmental criteria. The benefits of hydrogen production depend on the displaced

end-use, as different conversion factors are applied to quantify economic value and emission savings. In the first case study, hydrogen is assumed to replace conventional fuel in private vehicles.

3.2.1. Base Case Study

When hydrogen is produced for transportation, conversion factors are derived by comparing the costs and emissions of the displaced fuels. For a driving distance of 100 km, fuel consumption is estimated at 0.76 kgH_2 for a hydrogen vehicle (Toyota Mirai) [53], 6.8 L for a petrol vehicle [54], and 19.5 kWh for a battery electric vehicle (BEV) [55].

From an economic perspective, this corresponds to 8.95 L of petrol or 25.66 kWh of electricity saved per kilogram of hydrogen produced. Fuel prices are assumed to be 1.92 €/L for petrol (French average, January 2023) [56] and 0.147 €/kWh for home overnight charging [43]. This yields savings of 17.18 €/kgH_2 relative to petrol vehicles and 3.77 €/kgH_2 relative to BEVs.

In terms of emissions, petrol and electricity emission factors are taken as 2.8 $kgCO_2eq$/L [57] and 0.059 $kgCO_2eq$/kWh (French annual average) [39], respectively. Accordingly, hydrogen production avoids 25 $kgCO_2eq/kgH_2$ compared to petrol vehicles and 1.5 $kgCO_2eq/kgH_2$ compared to BEVs.

As these benefits depend on the vehicle types displaced, an assumption on fleet composition is required. The base case relies on a projected European vehicle fleet in 2040, with 30% electric vehicles [58]. Under this assumption, the resulting average conversion factors are 13.2 € and 18 $kgCO_2eq$ per kilogram of hydrogen produced.

Using these conversion factors, a multi-objective optimization is performed, and the resulting Pareto front is shown in Figure 9. The mono-objective optimum and three compromise solutions selected using LINMAP, TOPSIS, and GRA are reported in Table 12. As in the Power-to-Power case, the cost-optimal solution consists solely of a small PV system, indicating that PV-only configurations remain the only economically attractive option.

In contrast, from an emissions perspective, nearly all hydrogen-producing configurations yield substantial benefits. The optimization maximizes PV overproduction, with the electrolyzer sized to absorb this surplus within its operating limits. This indicates that emission reductions from hydrogen substitution largely outweigh the system's life-cycle greenhouse gas emissions. This configuration is hereafter referred to as OPT_ENV_2040.

Because the two objectives are strongly conflicting, cost minimization favoring small systems and emission minimization favoring large ones, Pareto-optimal solutions exhibit progressively reduced hydrogen system sizes. The selected compromise solutions lie close to the emission optimum. Both TOPSIS and GRA retain similar PV areas but reduce electrolyzer capacity, leading to only 2% and 6.6% lower hydrogen production, respectively, while substantially decreasing costs. Conversely, the LINMAP solution significantly reduces PV capacity, resulting in a pronounced drop in hydrogen production.

This case study demonstrates that hydrogen-based multi-energy systems can achieve competitive emission performance in a Power-to-Power configuration, although financial incentives remain necessary to ensure economic viability. However, these findings are strongly dependent on the conversion factors used to estimate the economic and environmental benefits of hydrogen production. Further work is therefore required to assess the robustness and general applicability of these results, which is addressed in the following section.

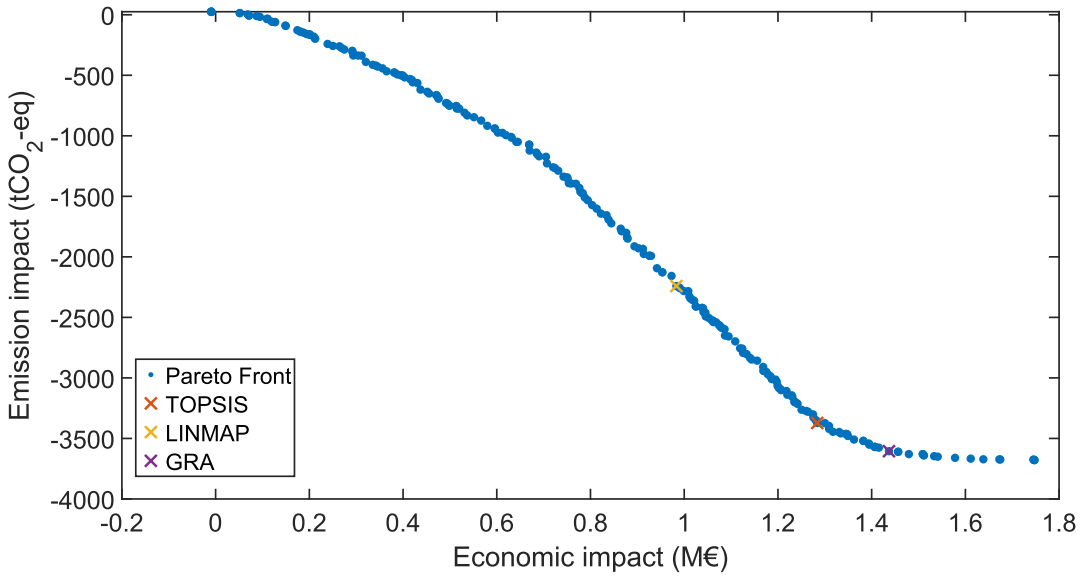

Figure 9 : Pareto front for the Power-to-Gas base case study

Table 12 : Selected configurations for the Power-to-Gas base case study

Component	**Cost optimum**	**LINMAP**	**TOPSIS**	**GRA**	**Emission optimum (OPT_ENV_2040)**
PV (monocrystalline)	215 m²	3676 m²	4968 m²	4979 m²	5000 m²
Electrolyzer (PEM)	0 kW	357 kW	528 kW	622 kW	753 kW
Hydrogen tank	0 kgH_2	54 kgH_2	69 kgH_2	80 kgH_2	107 kgH_2
NPC	-9 k€	983 k€	1284 k€	1437 k€	1747 k€
LCA Emission	25 tCO_2eq	-2241 tCO_2eq	-3372 tCO_2eq	-3605 tCO_2eq	-3679 tCO_2eq
Hydrogen produced annually	0 kgH_2	9.6 tH_2	14.1 tH_2	14.8 tH_2	15.1 tH_2

3.2.2. Variation of the conversion factors

To investigate the sensitivity of results to conversion factors within the transport application, the replaced vehicle fleet is varied. Three additional scenarios are considered: a fully petrol fleet, a fully electric vehicle (EV) fleet, and a fleet representative of the 2023 French mix (1.2% EVs) [59]. The corresponding conversion factors are summarized in Table 13. These factors decrease sharply with increasing EV penetration, reflecting the low electricity price and carbon intensity of the French grid

compared to the European average. This approach enables exploration of a broad range of conversion values.

Three additional multi-objective optimizations are conducted to assess how system design and performance evolve with these conversion factors. The resulting Pareto fronts are shown in Figure 10. The cost-optimal solution remains unchanged and consists solely of PV systems, indicating that for economic conversion factors below 17.2 €/kgH_2, hydrogen-based systems are not economically competitive.

The 100% petrol fleet and the 2023 fleet yield similar conversion factors and therefore comparable Pareto fronts. In contrast, the Pareto front for the 100% EV fleet collapses to a PV-only solution, as hydrogen production leads to higher costs and emissions than the baseline case (0 € and 0 tCO_2eq, corresponding to no system). The detailed configurations associated with the four Pareto fronts are presented in Figure 11. Although design trends remain consistent across all scenarios, performance levels vary substantially. Nevertheless, system sizes along the Pareto front remain largely unchanged, provided that configurations outperform the no-system reference point.

As in the Power-to-Power analysis, these results are strongly influenced by the decarbonized French electricity mix. To generalize the findings, system performance is evaluated under different electricity mixes, noting that the grid mix affects hydrogen substitution benefits, PV self-consumption, and balancing electricity costs. Using the OPT_ENV_2040 component sizes, performance is assessed in 26 European countries for the 100% EV fleet to determine whether this configuration remains uncompetitive. The results are shown in Figure 12. From an economic perspective, conclusions remain unchanged despite large inter-country variability. However, in terms of emissions, the system is not competitive with EVs in countries with highly decarbonized grids (e.g., France, Sweden, Belgium, Finland, and Spain), but achieves substantial emission reductions in 21 other countries.

In summary, these case studies indicate that hydrogen production for transport can be competitive in terms of emissions for current and projected 2040 vehicle fleets. However, it cannot outperform EV fleets supplied by low-carbon electricity (<60 gCO_2/kWh). As system sizing is weakly sensitive to conversion factors, further performance assessments can be conducted without repeating the computationally intensive multi-objective optimization.

Table 13 : hydrogen production conversion factors depending on the considered fleet of vehicles

vehicles	**Case 100% petrol**	**Case 2023**	**Case 2040**	**Case 100% electric**
Petrol-powered car (%)	100	98,8	70	0
electric car (%)	0	1,2	30	100
Economic rate (€ per kgH_2 produced)	17.2	17	13.2	3.77
Emission rate (kgCO_2eq per kgH_2 produced)	25.1	24.8	18	1.5

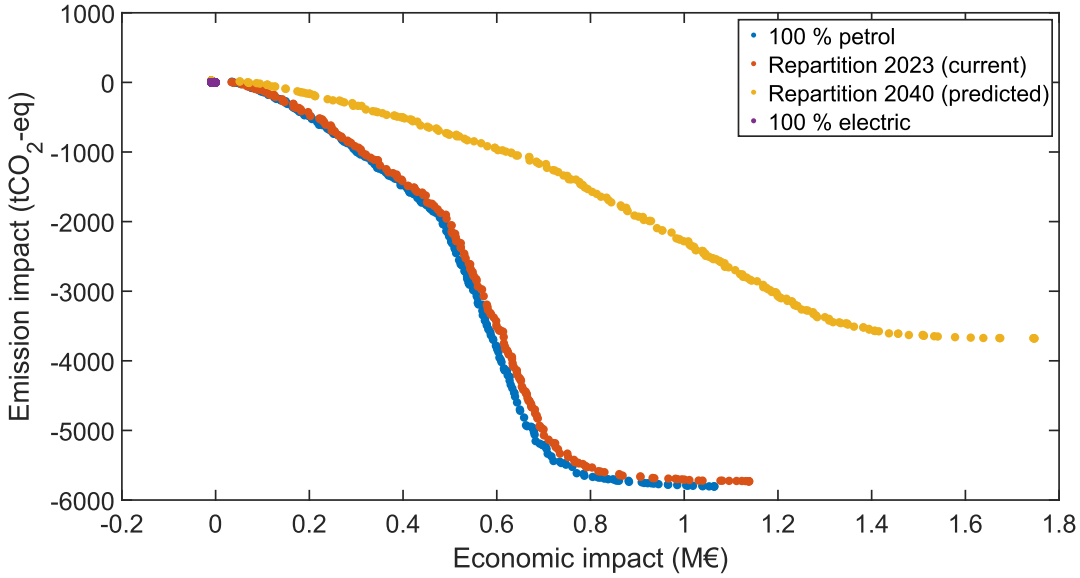

Figure 10 : Pareto front variation depending on hydrogen production conversion factors

Table 14 : Evolution of the emission optimum for the 4 vehicle fleets

Component	**Case 100% petrol**	**Case 2023**	**Case 2040**	**Case 100% EV**
PV (monocrystalline)	5000 m²	5000 m²	5000 m²	0 m²
Electrolyser (PEM)	724 kW	753 kW	753 kW	0 kW
Hydrogen tank	118 kg_{H2}	83 kg_{H2}	107 kg_{H2}	0 kg_{H2}
Economic impact	1064 k€	1139 k€	1748 k€	0 k€
Emission impact	-5806 tCO_2eq	-5732 tCO_2eq	-3679 tCO_2eq	0 tCO_2eq
Hydrogen produced annually	15.1 tH_2	15.1 tH_2	15.1 tH_2	0 tH_2

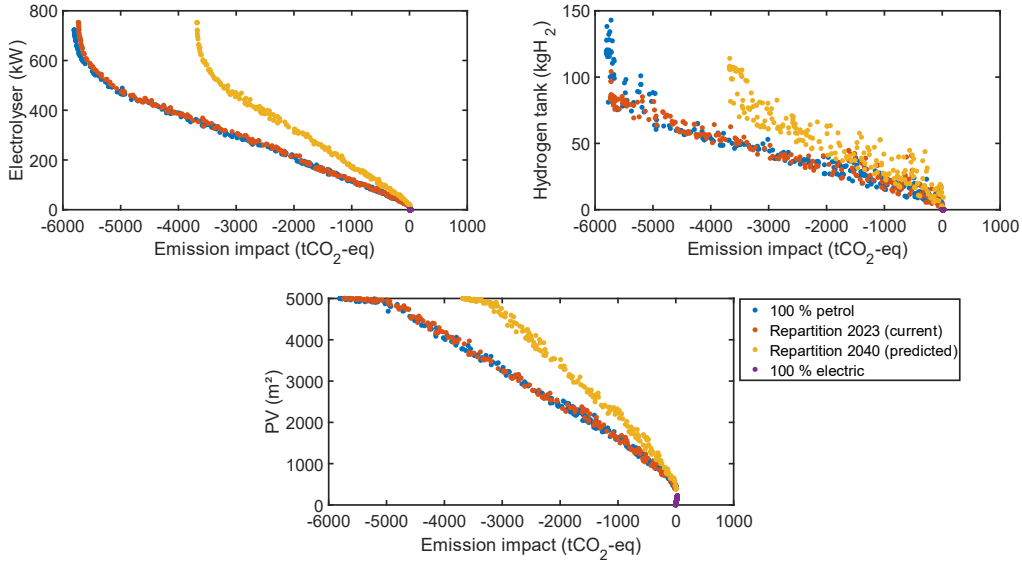

Figure 11 : Configuration inside the Pareto fronts (Power-to-Gas)

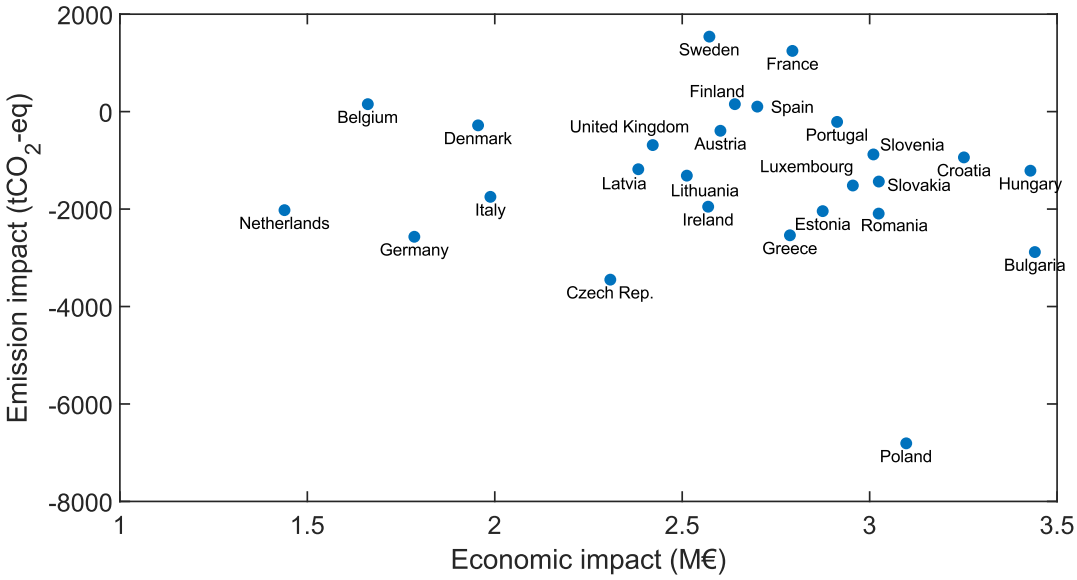

Figure 12 : Performance of the OPT_ENV_2040 configuration for a 100% EV Fleet in different European countries

3.2.3. Generalization to other hydrogen end-use

As previously observed, Pareto-optimal configuration sizes remain largely insensitive to variations in conversion factors. This stability allows the results to be generalized across multiple end uses.

To examine the economic performance of this architecture, the base-case (2040 fleet) configurations are considered. For each hydrogen-producing configuration, the hydrogen selling price required to achieve a net present cost of 0 € over 20 years is computed. This price corresponds to the break-even selling price. The results are presented in Figure 13. The lowest prices occur near the environmental

optimum, and generally decrease with increasing annual hydrogen production, until system oversizing leads to diminishing production gains.

The carbon intensity of the produced hydrogen is calculated as the ratio of the system's life-cycle greenhouse gas emissions to the total hydrogen produced over its lifetime. System emissions are defined as component life-cycle emissions minus emissions avoided through PV self-consumption. The resulting hydrogen carbon intensities for base-case optimized configurations are shown in Figure 14, converging toward approximately 6 $kgCO_2eq/kgH_2$.

These results indicate that economic competitiveness requires savings exceeding 22 $€/kgH_2$, while emission competitiveness requires savings greater than 6 $kgCO_2eq/kgH_2$ per kilogram of hydrogen produced. These thresholds can be compared with existing hydrogen production pathways. From an economic perspective, and as demonstrated in the transport case study, residential hydrogen production is not competitive without financial support. From an emissions standpoint, however, it can outperform conventional hydrogen production routes. Incer-Valverde et al. report carbon intensities between 7.5 and 25 $kgCO_2eq/kgH_2$ for hydrogen produced via steam methane reforming and coal gasification [60]. Therefore, any application currently relying on hydrogen from these processes could reduce its carbon emissions by using hydrogen produced from residential systems.

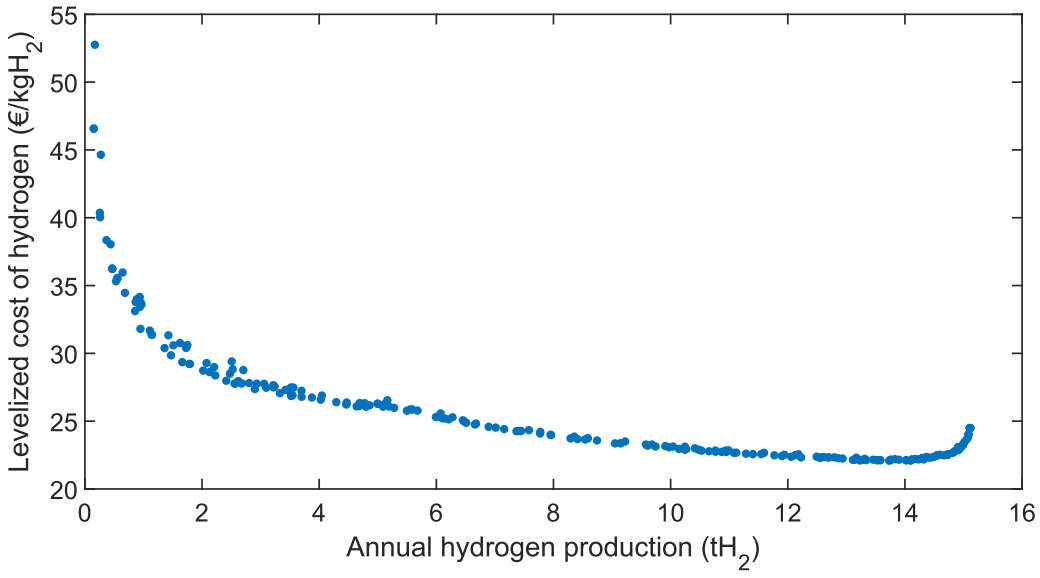

Figure 13 : Levelized cost of the hydrogen production in the Pareto front

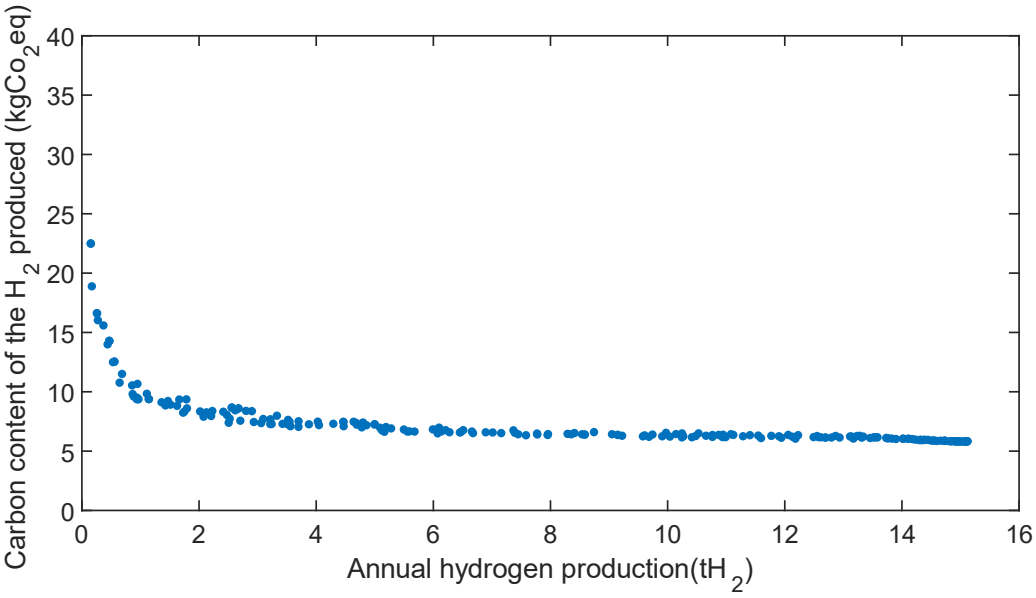

Figure 14 : Carbon content of the hydrogen production in the Pareto front

4. Conclusion

The objective of the present work is to evaluate and compare the potential of different hydrogen energy applications in residential environments, as well as to identify the sizing trends associated with each use. To achieve this, a flexible multi-energy model was implemented and applied in a multi-objective optimization. The system is optimized for two primary hydrogen energy applications in residential settings: hydrogen as a storage vector for PV overproduction (Power-to-Power) and hydrogen generation for sale (Power-to-Gas).

In the Power-to-Power case, results indicate that multi-energy systems using hydrogen storage are not currently competitive in terms of cost or greenhouse gas emissions compared to the French electricity grid. The system's main advantage is the renewable energy it provides. Economically, this conclusion holds even under high electricity cost scenarios, unless there is financial support. Environmentally, the results are strongly influenced by the low carbon intensity of the grid, and this outcome is specific to energy mixes heavily based on nuclear power (France) or hydroelectricity (Sweden), which are exceptions within the European Union. Transitioning the energy supply of residential buildings from low-carbon, non-renewable sources to renewable energy using hydrogen energy comes with significant trade-offs in terms of both cost and greenhouse gas emissions.

For the Power-to-Gas application, under the parameters used, the modeled hydrogen production has a carbon intensity of 6 to 10 kgCO_2eq per kilogram of hydrogen and a levelized cost of more than 20 € per kilogram. These orders of magnitude indicate that the system is not economically competitive without financial aid. In terms of life cycle emissions, the hydrogen produced can offer benefits in mobility applications, such as fuel for thermal or even electric vehicles, but only in regions with more carbon-intensive electricity grids than France. Moreover, the hydrogen produced could also be environmentally competitive for replacing hydrogen used in industry and generated from carbon-based processes.

Compared to the Power-to-Power application, the Power-to-Gas application offers better environmental performance because it displaces more carbon-intensive uses, such as transport and industrial processes. Nonetheless, the system remains economically challenging to make competitive without financial incentives.

Declaration of competing interest

The authors declare that they have no known competing financial interests or personal relationships that could have appeared to influence the work reported in this paper.

Acknowledgments

This work has been supported by the EIPHI Graduate School (contract ANR-17-EURE-0002) and the Region Bourgogne Franche-Comté.

Computations have been performed on the supercomputer facilities of the Mésocentre de calcul de Franche-Comté

Declaration of Generative AI and AI-assisted technologies in the writing process

During the preparation of this work, the authors used ChatGPT-4 and MistralAI-Medium to improve the grammar and readability of the manuscript. After using these tool/service, the authors reviewed and edited the content as needed and take full responsibility for the final publication.

5. Appendix A. Tariffs and carbon content of electricity networks in the European Union

Table 15 : Average annual tariff, carbon content and renewable energy proportion of electricity in European Union power grids

Country	**Rate (€/kWh) [51]**	**Carbon content (gCO_2eq/kWh) [39]**	**REP (%) [39]**
Austria	0.27	223	69
Belgium	0.44	169	23
Bulgaria	0.11	469	18
Croatia	0.15	277	28
Cyprus	0.37	820	15
Czech Rep.	0.32	525	14
Denmark	0.38	212	73
Estonia	0.22	386	38
Finland	0.26	169	48
France[1]	0.23	61	24
Germany	0.41	438	45
Greece	0.23	435	39
Hungary	0.12	304	19
Ireland	0.27	377	36
Italy	0.38	357	40
Latvia	0.31	301	48
Lithuania	0.28	314	42
Luxembourg	0.20	334	50
Netherlands	0.48	384	28
Poland	0.18	857	18
Portugal	0.21	205	63
Romania	0.19	391	42

Slovakia	0.19	326	19
Slovenia	0.19	271	41
Spain	0.25	174	49
Sweden	0.27	32	70
United Kingdom[2]	0.30	252	34

1: The French rate is higher than the one considered in the rest of the article to standardize the reference.

2 : Rates taken from the UK Department for Energy Security and Net Zero [61].

6. Appendix B. System energy management for the optimized sizes

The GRA method selects a small-scale configuration relative to the entire Pareto front. Its operation over three typical weeks is illustrated in Figure A-1. This configuration consists of a small PV area that generates very little excess production, approximately 78% of the photovoltaic production is absorbed by self-consumption. Of the remaining 22%, 10% is absorbed by the storage system and 12% is lost. Unlike the configurations presented earlier, hydrogen storage is not used here for long-term storage but cycles daily, just like a battery. The hydrogen loop therefore fulfills the same role as the battery, but only on days when solar irradiance is highest.

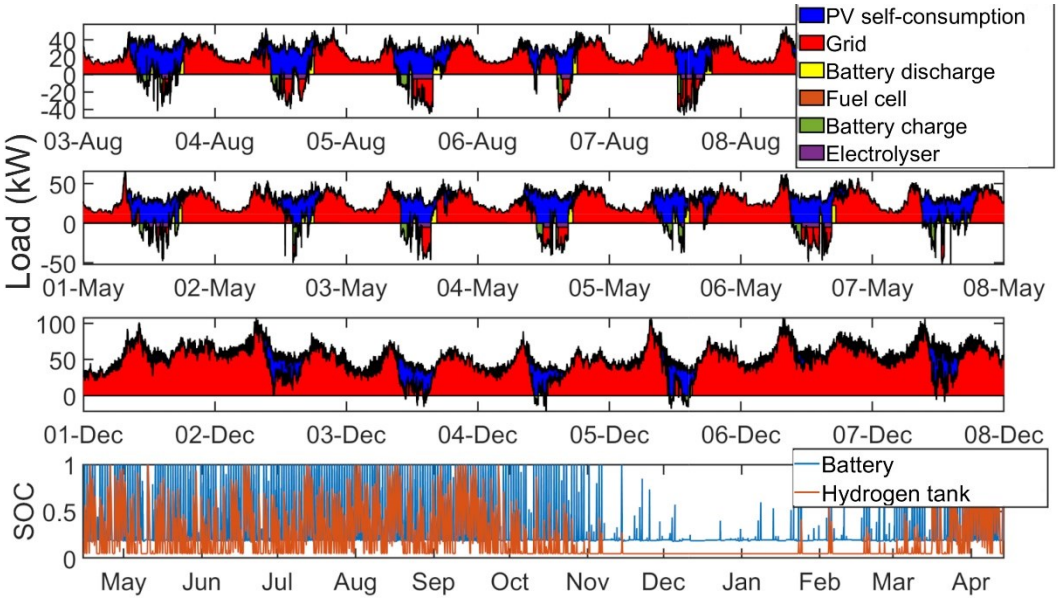

Figure A-1 : Multi-energy system yearly behavior in the P2P GRA optimum

In the configuration selected by the TOPSIS and LINMAP methods, a medium-capacity battery is used for daily energy storage, while the hydrogen loop enables seasonal energy storage. The operation of this configuration is illustrated in Figure A-2. The tank fills gradually between mid-April and early October and empties in the fall, from October through December. This corresponds to the storage of 42.2% of the photovoltaic energy, while 30.5% is directly used for self-consumption and 27,3% is lost. The chosen configuration does not allow for storing enough hydrogen for the entire winter and uses the hydrogen loop only for the first month of the heating season.

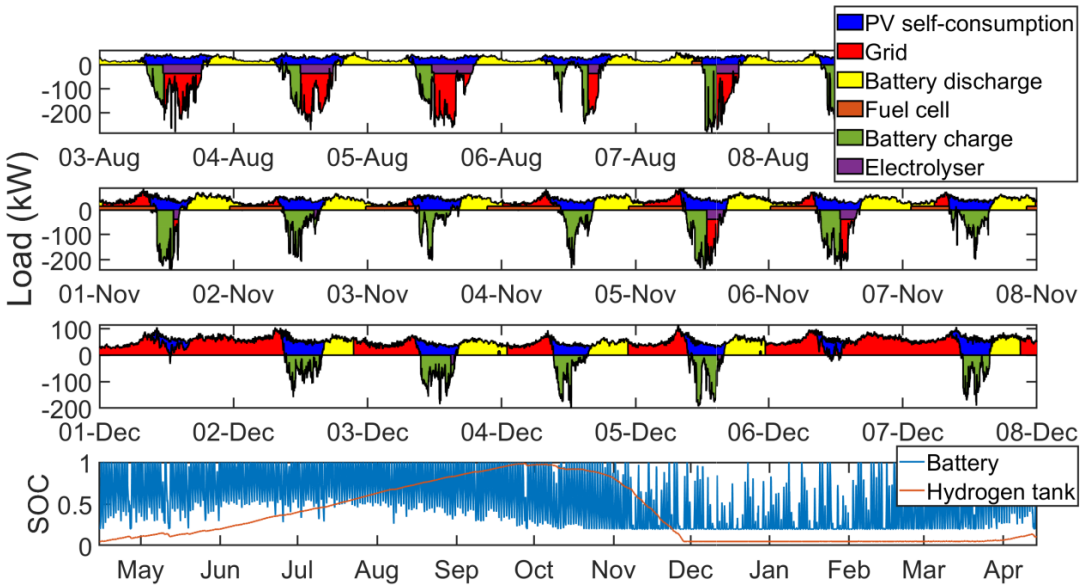

Figure A-2 : Multi-energy system yearly behavior in the P2P LINMAP/TOPSIS optimum

In the renewable energy optimum, very large components are selected. The surface area of photovoltaic panels is maximized to generate as much power as possible, regardless of the system's cost and life-cycle emissions. The system supplies the entire annual load through daily battery storage and seasonal storage using hydrogen systems. The operation of this configuration is illustrated in Figure A-3. Here, approximately 827 kWh of heat emitted by the fuel cell is lost, along with 21 MWh of solar energy and about 3.4 metric tons of hydrogen that go unused. In fact, while the other two indicators (cost and emissions) strike a balance between the system's size and its benefits to the buildings, the renewable energy proportion considers only the amount of energy the system provides. The energy factor therefore tends to result in an oversized system without any negative consequences. This objective function cannot, therefore, be used on its own and must always be adjusted by one of the other two.

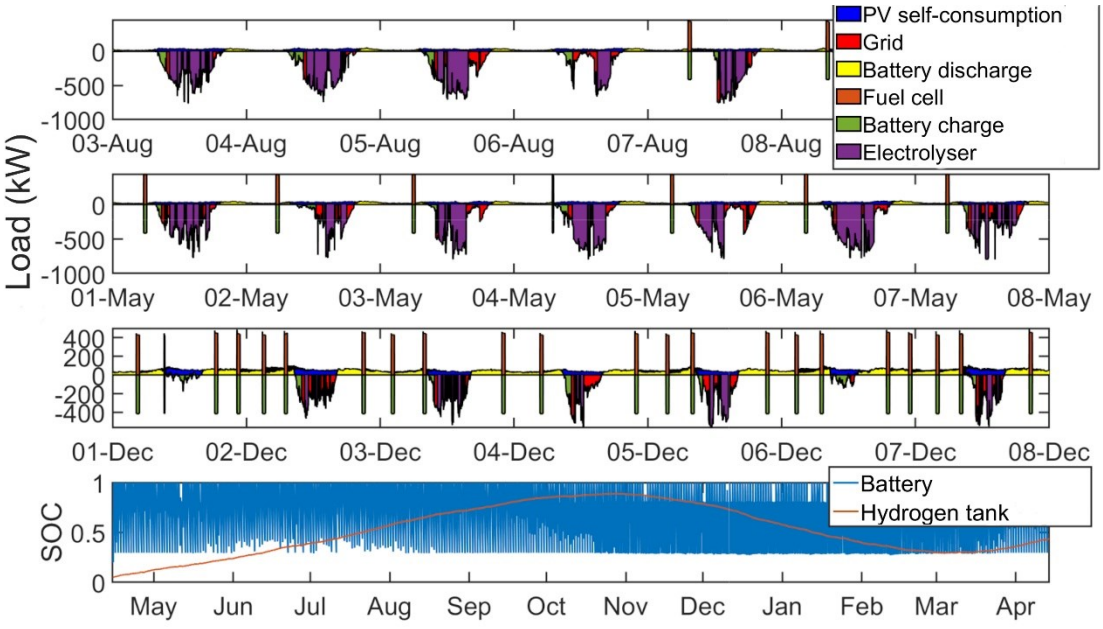

Figure A-3 : Multi-energy system yearly behavior in the P2P RES optimum

7. Bibliography

[1] International Energy Agency (IEA), "Tracking Clean Energy Progress 2023 - Buildings," Paris, 2023. [Online]. https://www.iea.org/reports/buildings.

[2] I. B. Mansir, E. H. B. Hani, H. Ayed and C. Diyoke, "Dynamic simulation of hydrogen-based zero energy buildings with hydrogen energy storage for various climate conditions," *International Journal of Hydrogen Energy,* vol. 47, pp. 26501-26514, 2022. https://doi.org/10.1016/j.ijhydene.2021.12.213.

[3] A. Mohammed, A. M. Ghaithan, A. Al-Hanbali and A. M. Attia, "A multi-objective optimization model based on mixed integer linear programming for sizing a hybrid PV-hydrogen storage system," *International Journal of Hydrogen Energy,* vol. 48, pp. 9748-9761, 2023. https://doi.org/10.1016/j.ijhydene.2022.12.060.

[4] C. Ghenai, T. Salameh and A. Merabet, "Technico-economic analysis of off grid solar PV/Fuel cell energy system for residential community in desert region," *International Journal of Hydrogen Energy,* vol. 45, p. 11460–11470, 2020. doi: 10.1016/j.ijhydene.2018.05.110.

[5] A. M. Ferrario, A. Bartolini, F. S. Manzano, F. J. Vivas, G. Comodi, S. J. McPhail and J. M. Andujar, "A model-based parametric and optimal sizing of a battery/hydrogen storage of a real hybrid microgrid supplying a residential load: Towards island operation," *Advances in Applied Energy,* vol. 3, p. 100048, 2021. https://doi.org/10.1016/j.adapen.2021.100048.

[6] O. M. Babatunde, J. L. Munda and Y. Hamam, "Hybridized off-grid fuel cell/wind/solar PV /battery for energy generation in a small household: A multi-criteria perspective," *International Journal of Hydrogen Energy,* vol. 47, pp. 6437-6452, 2022. https://doi.org/10.1016/j.ijhydene.2021.12.018.

[7] M. Kilic and A. F. Altun, "Dynamic modelling and multi-objective optimization of off-grid hybrid energy systems by using battery or hydrogen storage for different climates," *International Journal of Hydrogen Energy,* vol. 48, pp. 22834-22854, 2023. https://doi.org/10.1016/j.ijhydene.2022.12.103.

[8] K. Ou, W.-W. Yuan and Y.-B. Kim, "Development of optimal energy management for a residential fuel cell hybrid power system with heat recovery," *Energy,* vol. 219, p. 119499, 2021. doi: 10.1016/j.energy.2020.119499.

[9] P. Zhao, J. Wang, L. Gao and Y. Dai, "Parametric analysis of a hybrid power system using organic Rankine cycle to recover waste heat from proton exchange membrane fuel cell," *International Journal of Hydrogen Energy,* vol. 37, p. 3382–3391, 2012. doi: 10.1016/j.ijhydene.2011.11.081.

[10] H. Q. Nguyen, A. M. Aris and B. Shabani, "PEM fuel cell heat recovery for preheating inlet air in standalone solar-hydrogen systems for telecommunication applications: An exergy analysis," *International Journal of Hydrogen Energy,* vol. 41, p. 2987–3003, 2016. doi: 10.1016/j.ijhydene.2015.12.108.

[11] H. Lambert, R. Roche, S. Jemeï, P. Ortega and D. Hissel, "Combined Cooling and Power Management Strategy for a Standalone House Using Hydrogen and Solar Energy," *Hydrogen,* vol. 2, p. 207–224, 2021. doi: 10.3390/hydrogen2020011.

[12] D. C. Šanić and F. Barbir, "Stand-alone micro-trigeneration system coupling electrolyzer, fuel cell, and heat pump with renewables," *International Journal of Hydrogen Energy,* vol. 47, pp. 35068-35080, 2022. https://doi.org/10.1016/j.ijhydene.2022.08.090.

[13] M. Hosseini, I. Dincer and M. A. Rosen, "Hybrid solar-fuel cell combined heat and power systems for residential applications: Energy and exergy analyses," *Journal of Power Sources,* vol. 221, p. 372–380, 2013. doi: 10.1016/j.jpowsour.2012.08.047.

[14] P. Gabrielli, M. Gazzani, E. Martelli and M. Mazzotti, "Optimal design of multi-energy systems with seasonal storage," *Applied Energy,* vol. 219, pp. 408-424, 2018. https://doi.org/10.1016/j.apenergy.2017.07.142.

[15] P. Gabrielli, F. Fürer, G. Mavromatidis and M. Mazzotti, "Robust and optimal design of multi-energy systems with seasonal storage through uncertainty analysis," *Applied Energy,* vol. 238, pp. 1192-1210, 2019. https://doi.org/10.1016/j.apenergy.2019.01.064.

[16] J. Mustafa, S. Alqaed, F. A. Almehmadi, E. H. Malekshah and M. Sharifpur, "Effect of economic and environmental parameters on multi-generation of electricity, water, heat, and hydrogen in Saudi Arabia: A case study," *International Journal of Hydrogen Energy,* 2023. https://doi.org/10.1016/j.ijhydene.2023.07.035.

[17] M. Eldakadosi and J. Schneeloch, "Hydrogen vs. conventional sector-coupling residential energy systems: An economic and environmental comparison based on multi-objective design optimization," *Renewable Energy,* vol. 236, p. 121412, 2024. https://doi.org/10.1016/j.renene.2024.121412.

[18] G. Fambri, C. Diaz-Londono, A. Mazza, M. Badami, T. Sihvonen and R. Weiss, "Techno-economic analysis of Power-to-Gas plants in a gas and electricity distribution network system with high renewable energy penetration," *Applied Energy,* vol. 312, p. 118743, 2022. https://doi.org/10.1016/j.apenergy.2022.118743.

[19] L. M. Pastore, G. L. Basso, M. N. Quarta and L. de Santoli, "Power-to-gas as an option for improving energy self-consumption in renewable energy communities," *International Journal of Hydrogen Energy,* vol. 47, pp. 29604-29621, 2022. https://doi.org/10.1016/j.ijhydene.2022.06.287.

[20] J. D. Fonseca, J.-M. Commenge, M. Camargo, L. Falk and I. D. Gil, "Multi-criteria optimization for the design and operation of distributed energy systems considering sustainability dimensions," *Energy,* vol. 214, p. 118989, 2021. https://doi.org/10.1016/j.energy.2020.118989.

[21] F. Tooryan, H. HassanzadehFard, V. Dargahi and S. Jin, "A cost-effective approach for optimal energy management of a hybrid CCHP microgrid with different hydrogen production considering load growth analysis," *International Journal of Hydrogen Energy,* vol. 47, pp. 6569-6585, 2022. https://doi.org/10.1016/j.ijhydene.2021.12.036.

[22] S. Basnet, K. Deschinkel, L. L. Moyne and M. C. Péra, "Optimal integration of hybrid renewable energy systems for decarbonized urban electrification and hydrogen mobility," *International Journal of Hydrogen Energy,* vol. 83, pp. 1448-1462, 2024. https://doi.org/10.1016/j.ijhydene.2024.08.054.

[23] M. Armstrong, M. C. Swinton, H. Ribberink, I. Beausoleil-Morrison and J. Millette, "Synthetically derived profiles for representing occupant-driven electric loads in Canadian Housing," *Journal of Building Performance Simulation,* March 2009.

[24] M. Patin, S. Bégot, F. Gustin and V. Lepiller, "Enhancing Residential Sustainability: Multi-objective optimization of hydrogen-based multi-energy system," *International Journal of Hydrogen Energy,* vol. 67, pp. 875-887, 2024. https://doi.org/10.1016/j.ijhydene.2023.12.201.

[25] A. Arsalis, A. N. Alexandrou and G. E. Georghiou, "Thermoeconomic modeling of a completely autonomous, zero-emission photovoltaic system with hydrogen storage for residential applications," *Renewable Energy,* vol. 126, p. 354–369, 2018. doi: 10.1016/j.renene.2018.03.060.

[26] M. M. Samy, S. Barakat and H. S. Ramadan, "A flower pollination optimization algorithm for an off-grid PV-Fuel cell hybrid renewable system," *International Journal of Hydrogen Energy,* vol. 44, p. 2141–2152, 2019. doi: 10.1016/j.ijhydene.2018.05.127.

[27] M. A. Ancona, F. Catena and F. Ferrari, "Optimal design and management for hydrogen and renewables based hybrid storage micro-grids," *International Journal of Hydrogen Energy,* vol. 48, pp. 20844-20860, 2023. https://doi.org/10.1016/j.ijhydene.2022.10.204.

[28] M. Patin, S. Bégot, F. Gustin and V. Lepiller, *Bottom-up MATLAB generation algorithm of yearly energy consumption (electric and thermal) and photovoltaic production profiles for single-family houses in Central Europe,* 2023. [Online]. https://hal.science/hal-04574032.

[29] M. Yue, H. Lambert, E. Pahon, R. Roche, S. Jemei and D. Hissel, "Hydrogen energy systems: A critical review of technologies, applications, trends and challenges," *Renewable and Sustainable Energy Reviews,* vol. 146, p. 111180, 2021. https://doi.org/10.1016/j.rser.2021.111180.

[30] M. A. Khan, C. Young, C. Mackinnon and D. B. Layzell, "The Techno-Economics of Hydrogen Compression," 2021. [Online]. https://transitionaccelerator.ca/.

[31] G. Parks, R. Boyd, J. Cornish and R. Remick, "Hydrogen Station Compression, Storage, and Dispensing Technical Status and Costs," 2014. [Online]. https://www.nrel.gov/docs/fy14osti/58564.pdf.

[32] I. H. Bell, J. Wronski, S. Quoilin and V. Lemort, "Pure and Pseudo-pure Fluid Thermophysical Property Evaluation and the Open-Source Thermophysical Property Library CoolProp," *Industrial & Engineering Chemistry Research,* vol. 53, p. 2498–2508, 2014.

[33] M. R. Ranjbar and S. Kouhi, "Sources' Response for supplying energy of a residential load in the form of on-grid hybrid systems," *International Journal of Electrical Power & Energy Systems,* vol. 64, pp. 635-645, 2015. https://doi.org/10.1016/j.ijepes.2014.07.062.

[34] Danish Energy Agency, "Technology Data - Energy Plants for Electricity and District heating generation," 2016.

[35] C. Ghenai and M. Bettayeb, "Modelling and performance analysis of a stand-alone hybrid solar PV/Fuel Cell/Diesel Generator power system for university building," *Energy,* vol. 171, p. 180–189, 2019. doi: 10.1016/j.energy.2019.01.019.

[36] L. Gracia, P. Casero, C. Bourasseau and A. Chabert, "Use of Hydrogen in Off-Grid Locations, a Techno-Economic Assessment," *Energies,* vol. 11, 2018. doi: 10.3390/en11113141.

[37] A. Kirubakaran, S. Jain and R. K. Nema, "A review on fuel cell technologies and power electronic interface," *Renewable and Sustainable Energy Reviews,* vol. 13, pp. 2430-2440, 2009. https://doi.org/10.1016/j.rser.2009.04.004.

[38] O. Gudmundsson, J. Thorsen and L. Zhang, "Cost analysis of district heating compared to its competing technologies," 2013.

[39] Electricity maps, *Electricity maps Database,* 2022. [Online]. https://www.electricitymaps.com/.

[40] OECD, *Inflation (CPI) (indicator),* 2024.

[41] Clean Hydrogen Partnership, "Strategic Research and Innovation Agenda 2021-2027," 2022. [Online]. https://www.clean-hydrogen.europa.eu/about-us/key-documents/strategic-research-and-innovation-agenda_en.

[42] Réseau européen des gestionnaires de réseau de transport d'électricité (ENTSO-E), *ENTSO-E transparency platform, Day-ahead Prices,* 2024.

[43] Commission de régulation de l'énergie (CRE), *Historique des tarifs réglementés de vente d'électricité pour les consommateurs résidentiels, Option heures pleines heures creuses,* 2024. [Online]. https://www.data.gouv.fr/fr/datasets/r/f7303b3a-93c7-4242-813d-84919034c416.

[44] H. Bahlawan, W.-R. Poganietz, P. R. Spina and M. Venturini, "Cradle-to-gate life cycle assessment of energy systems for residential applications by accounting for scaling effects," *Applied Thermal Engineering,* vol. 171, p. 115062, 2020. https://doi.org/10.1016/j.applthermaleng.2020.115062.

[45] V. Knop, *Life Cycle Analysis of hydrogen compression,* 2022. [Online]. https://www.awoe.net/Hydrogen-Compression-LCA.html.

[46] R. Frischknecht, R. Itten, F. Wyss, I. Blanc, G. Heath, M. Raugei, P. Sinha and A. Wade, "Life Cycle Assessment of Future Photovoltaic Electricity Production from Residential-scale Systems Operated in Europe," 2014. [Online]. https://iea-pvps.org/key-topics/iea-pvps-task-12-life-cycle-assessment-of-future-photovoltaic-electricity-production-from-residential-scale-systems-operated-in-europe-2015/.

[47] D. Bionaz, P. Marocco, D. Ferrero, K. Sundseth and M. Santarelli, "Life cycle environmental analysis of a hydrogen-based energy storage system for remote applications," *Energy Reports,* vol. 8, pp. 5080-5092, 2022. https://doi.org/10.1016/j.egyr.2022.03.181.

[48] Argonne National Laboratory, *GREET2,* 2022. [Online]. https://greet.es.anl.gov/.

[49] Agence de l'environnement et de la maîtrise de l'énergie (Ademe), "Analyse de cycle de vie relative à l'hydrogène, Production d'hydrogène et Usage en mobilité légère," 2020.

[50] Z. Wang and G. P. Rangaiah, "Application and Analysis of Methods for Selecting an Optimal Solution from the Pareto-Optimal Front obtained by Multiobjective Optimization," *Ind. Eng. Chem. Res.,* vol. 56, p. 560–574, January 2017.

[51] Eurostat, *Electricity prices for household consumers - bi-annual data (from 2007 onwards),* 2024. [Online]. https://ec.europa.eu/eurostat/databrowser/view/nrg_pc_204/default/table?lang=en.

[52] H. Ritchie and P. Rosado, "Electricity Mix," *Our World in Data,* 2020. [Online]. https://ourworldindata.org/electricity-mix.

[53] H2.live, *Hydrogen vehicles, All models at a glance,* 2024. [Online]. https://h2.live/en/fcev/.

[54] Agence de l'environnement et de la maîtrise de l'énergie (Ademe), *Évolution de la consommation moyenne, Véhicules particuliers neufs vendus en France,* 2024. [Online]. https://carlabelling.ademe.fr/chiffrescles/r/evolutionConsoMoyenne.

[55] Electric Vehicule Database, *Energy consumption of full electric vehicles.*

[56] Institut national de la statistique et des études économiques (INSEE), *Prix moyens mensuels de vente au détail en métropole - Gazole (1 litre),* 2024. [Online]. https://www.insee.fr/fr/statistiques/serie/000442588#Tableau.

[57] Ministère de l'Écologie, du développement durable et de l'Énergie, "GHG information for transport services - Application of Article L. 1431-3 of the French transport code - Methodological guide," 2019.

[58] J. Neuhausen, J.-H. Bomke, P. Rose, M. Wietschel, P. Plötz, S. Link, F. Ferk and T. Gnann, "European Fleet Electrification - From Electric Vehicle Sales to a complete Fleet Transition,," 2023.

[59] Ministère de la Transition écologique et de la Cohésion des territoires, "Données sur le parc automobile français au 1er janvier 2023,," 2023. [Online]. https://www.statistiques.developpement-durable.gouv.fr/donnees-sur-le-parc-automobile-francais-au-1er-janvier-2023.

[60] J. Incer-Valverde, A. Korayem, G. Tsatsaronis and T. Morosuk, "“Colors” of hydrogen: Definitions and carbon intensity," *Energy Conversion and Management,* vol. 291, p. 117294, 2023. https://doi.org/10.1016/j.enconman.2023.117294.

[61] UK Department forEnergy Security and Net Zero, *Average variable unit costs and fixed costs for electricity for regions in the United Kingdom,* 2023.

[62] H. Tao, K. A. Mamun, A. Ali, E. Solomin, J. Zhou and N. Sinaga, "Performance enhancement of integrated energy system using a PEM fuel cell and thermoelectric generator," *International Journal of Hydrogen Energy,* 2023. https://doi.org/10.1016/j.ijhydene.2023.03.442.

[63] S. Ham, D. Park, W.-Y. Lee and M. Kim, "Simulation to analyze operation strategy of combined cooling and power system using a high-temperature polymer electrolyte fuel cell for data centers," *International Journal of Hydrogen Energy,* vol. 48, pp. 8247-8259, 2023. https://doi.org/10.1016/j.ijhydene.2022.11.257.

[64] International Energy Agency (IEA), "Tracking Clean Energy Progress 2023 - District Heating," Paris, 2023. [Online]. https://www.iea.org/reports/buildings.

[65] Y. Qin, H. Zhang and X. Zhang, "Integrating high-temperature proton exchange membrane fuel cell with duplex thermoelectric cooler for electricity and cooling cogeneration," *International Journal of Hydrogen Energy,* vol. 47, pp. 38703-38720, 2022. https://doi.org/10.1016/j.ijhydene.2022.09.041.

[66] F. Musharavati and S. Khanmohammadi, "Performance improvement of a heat recovery system combined with fuel cell and thermoelectric generator: 4E analysis," *International Journal of Hydrogen Energy,* vol. 47, pp. 26701-26714, 2022. https://doi.org/10.1016/j.ijhydene.2021.09.179.

[67] P. Murray, J. Marquant, M. Niffeler, G. Mavromatidis and K. Orehounig, "Optimal transformation strategies for buildings, neighbourhoods and districts to reach CO2 emission reduction targets," *Energy and Buildings,* vol. 207, p. 109569, 2020. https://doi.org/10.1016/j.enbuild.2019.109569.

[68] Y. Han, G. Zhang, Q. Li, Z. You, W. Chen and H. Liu, "Hierarchical energy management for PV/hydrogen/battery island DC microgrid," *International Journal of Hydrogen Energy,* vol. 44, p. 5507–5516, 2019. doi: 10.1016/j.ijhydene.2018.08.135.

[69] J. Romdhane, H. Louahlia and M. Marion, "Dynamic modeling of an eco-neighborhood integrated micro-CHP based on PEMFC: Performance and economic analyses," *Energy and Buildings,* vol. 166, pp. 93-108, 2018. https://doi.org/10.1016/j.enbuild.2018.01.054.

[70] J. J. Hwang and M. L. Zou, "Development of a proton exchange membrane fuel cell cogeneration system," *Journal of Power Sources,* vol. 195, pp. 2579-2585, 2010. https://doi.org/10.1016/j.jpowsour.2009.10.087.

[71] P. Corbo, F. Migliardini and O. Veneri, "Experimental analysis and management issues of a hydrogen fuel cell system for stationary and mobile application," *Energy Conversion and Management,* vol. 48, pp. 2365-2374, 2007. https://doi.org/10.1016/j.enconman.2007.03.009.

[72] W. Marion and K. Urban, "User's Manual for TMY2s (Typical Meteorological Years)-Derived from the 1961-1990 National Solar Radiation Data Base," 1995.